INVESTIGATION OF TWO KINETIC PROBLEMS IN METALLURGY

A thesis submitted
in Partial Fulfilment of the Requirements
for the degree of

MASTER OF TECHNOLOGY

[illegible]

BY

DEEPAK KUMAR SENGUPTA

to the

DEPARTMENT OF METALLURGICAL ENGINEERING

INDIAN INSTITUTE OF TECHNOLOGY, KANPUR

JULY, 1984

22 AUG 1984

CENTRAL LIBRARY

Acc. No. A 83735

ME-1984-M-SEN-INV

DEDICATED

TO

MY PARENTS

AS A MARK OF AFFECTION

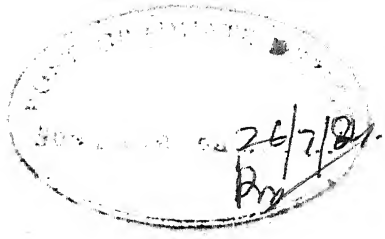

CERTIFICATE

Certified that the work entitled 'Investigation of two Kinetic Problems in Metallurgy' by D.K. SENGUPTA has been carried out under my supervision and has not been submitted elsewhere for a degree.

JULY, 1984.

DR. A.K. JENA
PROFESSOR AND HEAD
DEPT. OF METALLURGICAL ENGG.
INDIAN INSTITUTE OF TECHNOLOGY,
KANPUR.

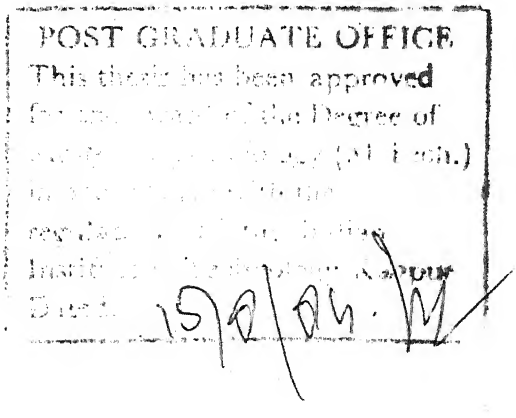

ACKNOWLEDGEMENTS

At the outset, I wish to express my deep sense of graditude to Prof. A.K. JENA for his valuable guidance. I am highly grateful to him for his understanding, keen encouragement, Kind help extended to me in carrying out the Project.

It is impossible to fully appreciate in words the warmth and affection that my innumerable friends accorded to me throughout the period of my stay here.

I personally thank all the people who have associated with me in all dimensions and in all spaces.

- D.K. SENGUPTA

TABLE OF CONTENTS

		PAGE
CERTIFICATE		iii
ACKNOWLEDGEMENT		iv
TABLE OF CONTENTS		v
LIST OF FIGURES		vii
LIST OF TABLES		ix
ABSTRACT		x
CHAPTER 1 :	INTRODUCTION	1
CHAPTER 2 :	LITERATURE REVIEW	3
2.1	Kinetics of Precipitation in Ni-base Superalloy	3
2.2	Precipitation in Ni-CO-Cr-Nb-V Alloys	8
2.2.1	Microstructure	9
2.3	Reduction of FeO by CO	11
2.4	Potential Energy Curves and the Activated State	11
2.5	Construction of Potential-Energy Surfaces Semiempirical Method	13
2.6	Concluding Remarks	16
CHAPTER 3 :	EXPERIMENTAL PROCEDURE FOR RESISTOMETRIC STUDY OF PRECIPITATION IN Ni-CO-Cr-Nb-V SUPERALLOY	17
3.1	Material	17
3.2	Processing of Material	17
3.3	Electrical Resistivity Measurements	19

PAGE

		3.3.1 Sample Preparation	19
		3.3.2 Experimental Set-up	19
		3.3.3 Measurement Technique	21
CHAPTER	4 :	RESULTS AND DISCUSSION OF PRECIPITATION KINETICS IN THE NICKEL BASE ALLOY	24
	4.1	Variation of Resistivity With Time	24
	4.2	Precipitate Sequence in the Ni-Base Alloy	25
	4.3	Kinetics of Precipitation	26
	4.4	A Kinetic Model	29
CHAPTER	5 :	ATOMIC MECHANISM OF REACTIONS INVOLVED IN REDUCTION OF FeO BY CO	32
	5.1	General	32
	5.2	A Physical Model	32
	5.3	Change of Energy of this System	35
		5.3.1 Bonding Between Two Atoms	35
	5.4	Morse Potential	36
	5.5	Physical Segnificance of α	40
	5.6	Energy of Formation of CO_2	42
	5.7	Activation Energy for the Formation of of CO_2 from CO and O	45
CHAPTER	6 :	SUMMARY AND CONSLUSIONS	46
APPENDIX	A :	COMPUTER PROGRAM FOR POTENTIAL ENERGY PLOT OF CO	78
	B :	COMPUTER PROGRAM FOR RESISTOMETRIC ANALYSIS USING LEAST SQUARE METHOD	79
	C :	COMPUTER PROGRAM FOR POTENTIAL ENERGY SURFACE PLOT OF CO_2 USING BISECTION METHOD	83
	D :	COMPUTER PROGRAM FOR POTENTIAL ENERGY SURFACE PLOT OF Fe-O-C-O USING BISECTION MET	84
REFERENCES			

LIST OF FIGURES

FIGURE NO.	CAPTION	PAGE
1	Hardness Ageing Curves for Alloy at 650 °C, 750 °C and 850 °C	52
2	Structure of Alloy Aged for 1 Hour at 650 °C	53
3	Structure of Alloy Aged for 1 Hour at 850 °C	54
4	Structure of Alloy Aged for 3 Hours at 750 °C	55
5	Structure of Alloy Aged for 1039 Hours at 750 °C	56
6	Structure of Alloy Aged for 1039 Hours at 650 °C	57
7	Variation of Potential Energy Accompanying the Reaction $X+YZ = XY+Z$	58
8	Typical Potential Energy Surface for Three Atom Reaction	58
9	Profile of Reaction Path	58
10	Schematic Setup for Measuring Resistivity of the Sample	59

FIGURE NO.	CAPTION	PAGE
10a	Variation of Resistivity with Ageing Time at 600, 625 and 650 °C	60
10b	Variation of Resistivity With Ageing Time at 750 °C and 850 °c	61
10c	Structure of Alloy Aged for 50 Hours at 750 °C	62
10d	Dark Field Structure of γ" Precipitates Present in Fig. 10c	63
11a	Factors Contributing to Resistivity Change	64
11b	Factors Contributing to Resistivity Change	64
12a	FeO Unit Cell	65
12b	Interaction of FeO Lattice with Co Molecule	65
13	Bonding Between two Atoms -Nature of Force	66
14	Bonding Between two Atoms-Nature of Energy	67
15	Potential Energy Curve for Diatomic Molecule	68
16	Potential Energy Contours for Formation of CO_2 from CO and O.	69
17	Activation Energy Plot for CO_2	70

LIST OF TABLES

TABLE NO.	TITLE	PAGE
1	Resistivity of Solution Treated Sample	71
2	Resistivity of Aged Samples	72
3	Resistometric Analysis Parameters Fitting of Equation(8) Chapter 4	77

ABSTRACT

Two typical kinetic problems in metallurgy have been analyzed in order to obtain information on their atomic mechanisms. A 34.9 wt. % Ni - 34.9 Wt. % Co - 14.2 Wt. % Cr - 8 Wt. % Nb - 8 Wt. % V alloy was homogenized and aged at 600, 625 , 650, 750 and 850 °C upto 100 hours and the change in resistivity was measured. The change in resistivity increases with time and attains a maximum due to ageing at 600, 625 and 650 °C. The $\Delta\rho$ value at 850 °C first decrease and then increase with time and at 750 °C $\Delta\rho$ against ageing time curve is like the low temperature curves upto 30 minutes when it suddently changes its behaviour to that observed for samples aged at 850 °C. It has been shown that at 600, 625 and 650 °C γ'' precipitates whereas at 850 °C β precipitates. 750 °C leads to precipitation of γ'' at the early stage and β at the later stages. Computer calculations based on these results show that the atomic model proposed by White et al is not applicable to these alloys.

A model for reduction of FeO by CO and formation of Fe and CO_2 was considered. Using morse potential the potential energy of CO and the potential energy surface of CO_2 were calculated. The calculated value of energy of dissociation

of CO_2 to CO and O is + 325 K Cal which compares well with the thermodynamic value of + 381 K Cal. The activation energy was found to be 22 K Cal. The potential energy calculations for Fe-O-C-O system however was not very safisfactory. This was primarily because considerable more work need to be done in order to take into account the interaction with solid FeO.

CHAPTER 1

INTRODUCTION

One of the major developments recently made in the scientific world has been the perfection of the electronic computers in both its analog and digital form. The utility of electronic computers in the engineering of metallurgical systems is now well established, and computers undoubtedly will take preeminence as a tool of the research endeavour. Computers are used presently in research and in operating practice for a variety of applications involving metallurgical calculations and data analysis. Computer applications involving simulation and control of metallurgical processes are rapidly expanding, furthermore, the storage and retrieval of metallurgical information is a subject of increasing importance.

The purpose of the present work is to outline computer applications to two metallurgical processes which can be easily experimentally handled.

a) Kinetics of precipitation in a nickel-base super-alloy.

b) Kinetics of reduction of FeO.

Computer application to the above two kinetics studies leads to the study of the atomic mechanisms of the two processes.

The aim of the first part of the work is to understand the kinetics of a reduction reaction and also to determine

using the reaction path analysis the activation energy of the reduction reaction. The activation energy of the activated complex formed prior to product stage is calculated using the principles of potential energy surface.

The second part of the work investigate the precipitation characteristics of the Ni-Cr-Co-Nb alloy containing vanadium. It leads to an understanding of the nature of the precipitates formed after various heat treatments.

CHAPTER 2

LITERATURE REVIEW

1. INTRODUCTION

It was stated in the last chapter that two kinetic problems have been examined in this investigation. In this chapter available literature related to the two topics are briefly reviewed.

2.1 Kinetics of precipitation in Ni-base superalloy

Superalloys are now widely used in a variety of applications at temperature ranging from 923 to 1373°K in aggressive atmospheres such as combustion products of fuel and air, high temperature catalytic reactors etc. In order to function satisfactorily in such a severe environment superalloys must possess properties such as outstanding high temperature strength, creep and fatigue resistance, excellent ductility, good impact resistance and adequate resistance to hot - corrosion (1).

Superalloys are essentially of three types, iron-base, nickel-base and cobalt-base (1). We would be primarily concerned with Ni-base alloys. Nickel-base superalloys consist of primarily nickel containing number of solutes such as Cr, Co, Mo, W etc. Chromium and cobalt increases the corrosion

resistance and the rest change the matrix stability and matrix strength. Small amounts of carbon is always present which gives rise to carbides at the grain boundaries and increases the high-temperature fatigue resistance. Suitable heat-treatments are imparted in order to have desired distribution of the carbides. However, the strength of these alloys is primarily due to the precipitation of inter-metallic compounds of the type Ni_3X where X stands for suitable solute.

The precipitates increase the resistance to dislocation motion. Dislocations may either bow around the precipitate or cut through them. The stress necessary for the dislocations to bow around precipitates is inversely proportional to the inter-particle distance which increase with increase in particle size in a system which has a fixed volume fraction of the precipitations phase. The stress required to cut the precipitates is proportional to the square-root of its size. Hence the optimum strength is obtained when the inter-particle spacing is just small enough to prevent the dislocations from bowing. The characteristics which determine the magnitude of stress required to cut the precipitate are: elastic coherency strains around the precipitate, antiphase boundary energy of ordered precipitate, precipitate-matrix interfacial energy and the difference between the elastic-modui and stacking - fault energy of precipitate and matrix (2).

A number of elements form Ni_3X type compounds the compounds in the Ni-base binary systems containing Mn, Fe, Co and pt are formed at low temperatures as a result of ordering reactions. High temperature strengthening due to precipitation in these systems is therefore unlikely. The rest of the solutes Al, Ti, V, Nb, Ta, Mo, Ga, IN, Si, Ge and Sn form Ni_3X type compounds which are stable upto relatively high temperatures. Amongst all these compounds only Ni_3V forms by ordering and the rest are formed by peritectic or peritectoid reaction. The solubilities of these compounds in nickel decrease rapidly with decrease in temperature. These alloys are therefore, likely to be suitable for precipitation.

The compounds Ni_3Al, Ni_3Ga and Ni_3Ge are ordered cubic (LI_2). Ni_3Ti has an ordered hexagonal structure (DO_{24}). Ni_3In and Ni_3Sn are also ordered hexagonal but then c-axis is nearly half of that of Ni_3Ti. Ni_3V and the high temperature modification of Ni_3Ta are ordered Tetragonal (DO_{22}). The structure of Ni_3Nb, the low temperature modification of Ni_3Ta and Ni_3MO are ordered orthorhombic (Cu_3Ti) (3).

The arrangement of atoms in FCC nickel (Al) is identical with that in the LI_2 structure if ordering in the later is ignored. The close-packed planes (111) are stacked in both in the same sequence, ABC. The hexagonal unit cell of DO_{24} structure may be ccnsidered as four HCP unit cells stacked on

four others such that the lattice parameters of DO_{24} are twice the corresponding lattice parameter of HCP cells. Thus the close-packed (001) plane of DO_{24} is similar to the (111) plane of FCC nickel. The hexagonal unit cell of DO_{19} structure consist of four HCP unit cells placed next to each other such that the lattice parameter "a" of DO_{19} is twice that of HCP structure. The planes of atoms parallel to (001) are similar to the (111) planes of FCC. The DO_{22} consist of the FCC unit cells stacked one above the other. The (112) plane of DO_{22} has the same arrangement of atoms at the (111) plane of nickel. If slight distortion is ignored the atomic arrangements in the (010) plane of the Cu_3Ti structure becomes same as that in the (111) plane of nickel.

The arrangements of atoms in the (111), (001), (112) and (010) planes of LI_2, DO_{24}, DO_{19}, DO_{22} and Cu_3Ti type structures is the same as that in the (111) plane of nickel. Similarly (001) planes of nickel are similar to the (001) planes of LI_2 and (100) and (001) planes of DO_{22} (3).

The close similarity between the atomic arrangements in various planes gives rise to the formation of coherent interface between the nickel rich matrix and the precipitating compounds.

Coherent interface between precipitates and matrix may lead to appreciable strengthening. Relatively small coherency strains and low surface energies associated with coherent

precipitates result in uniform distribution of precipitates and high resistances to coarsening. The formation of coherent precipitate is encouraged by small mismatch. The shapes of precipitates are related to strain-energy. The magnitude of strain energy is determined by mismatch, orientation and size of the precipitate.

The alloying elements substitute for both nickel and X in Ni_3X. Substitution of Ni in Ni_3X by CO, Fe, Cr, Mo and W results in an increase in the lattice parameter of Ni_3X cancelling partly their effect in reducing the mismatch by increasing the lattice parameter of the matrix. Cr, Fe, Mo and W substitute for X in Ni_3X to a minor extent. Therefore, their effect on the mismatch due to change in the lattice parameter of Ni_3X would not be appreciable. Change in the lattice parameter of Ni_3X due to substitution of X by Al, Ti, V, Ta, Nb, Ga, IW, Ge, Si and Sn would depend upon their relative atomic diameters.

Substitution of Al in Ni_3Al by Ti or Nb leads to an increase in the lattice parameter of γ'. Substitution of V and Si for Al leads to a decrease in the lattice parameter of Ni_3Al (4,5).

The elements decreasing the lattice parameter of Ni_3X would generally reduce the mismatch.

The microstructure of a precipitation hardened system consists of precipitates of different sizes distributed in the matrix. The smaller precipitate have much higher surface to volume ratios than the larger ones and hence the free energy per unit volume of a smaller precipitate and its solubility in the matrix are higher than those of bigger precipitate. Suitable alloying elements can be substituted in order to improve stability of precipitates.

2.2 Precipitation in Ni-Co-Cr-Nb-V Alloys

The influence of the addition of vanadium on the precipitation behaviour of Ni-Co-Cr-Nb alloys has been examined (6). In this investigation the specimen was solution treated at 1423°K, water quenched and then aged at 923, 1023, and 1123°K for various lengths of time. The aging kinetics were followed by hardness measurements and structural studies was conducted by TEM techniques.

The variation in hardness with ageing time of the alloy at various ageing temperature is shown in fig. (1). It is to be noted that as the ageing temperature is reduced the hardness value of the peak aged specimens is increased and the time required to achieve peak hardness is also increased. At 923 K, however, the peak hardness was not attaind even after 1039 hours of ageing.

At the ageing temperature of 1023°K the ageing curve seems to reach a plateau after an initial hardness increase of 60% and before continuing to increase further. Such behaviour suggests possible presence of a two stage precipitation process.

2.2.2 Microstructure

The structure of the solution treated specimen was single phase FCC. The lattice parameter of the alloying was determined by X-ray diffractometry to be 3.594 A°. Comparison of this value with the lattice parameter of the alloy containing 37% Ni, 38% CO, 17% Cr and 8% Nb by weight (a = 3.556 A°) (7) and of the r" phase (a = 3.600 A°) (7) suggests that addition of vanadium tends to increase the lattice parameter of the matrix and reduce the mismatch with r".

During the early stages of ageing at 923 K discrete precipitate particles could not be seen in the structure of a specimen aged for 1 hour at 923 fig. (2). The mottled surface observed in fig. (2) can be attributed to the coherency strains around r" precipitate particles. The specimen did not reveal the presence of any other type of precipitate, but stacking fault were present. These stacking faults did not have any precipitate particles associated with them.

The effect of increasing the ageing temperatures was to increase the rate of precipitation appreiably as demonstrated by the microstructure of the specimen aged for one hour at

1123 K in fig. (3). This figure also shows that in addition to γ", lath shaped precipitate and stacking fault are also present in this specimen. The lath shaped precipitates were identified with the help of diffraction patterns as equilibrium orthorhombic β phase which formed on the (111) matrix planes. No precipitates was observed in association with the stacking fault. The microstructure of the specimen aged for one hour at 1023 was similar but contained a fewer number of laths of β.

An increase in ageing time coarsened the γ" precipitates and encouraged or increased the formation of precipitates. As illustrated in figure (4), the structure of a specimen aged for 3 hours at 1023 K consists predominately of γ" phases with a few laths of β phase. The grain boundary precipitates are also identified as β. Precipitates free zones around them and around the laths of β within the matrix are observed. After 1039 hrs of ageing only laths of orthorhombic β phase were present.(5). However, at 923K a large amount of γ" was still present even after 1039 hrs of ageing fig. (6).

The results of the investigation demonstrate that the addition of vanadium to Ni-Co-Cr-Nb alloys promotes the precipitation of metastable phase γ". One hour of ageing at 923 K is enough to produce precipitates of only γ" phase. An increase in the time and temperature of ageing the alloy result

in precipitation of lath-shaped equilibrium phase β and upon continued ageing upto 1039 hours at 1023 K γ'' phase dissappeared completely and only β phase remains. The two stage ageing behaviour suggested by the hardness ageing time curve at 1023 K figure (1) can be attributed to the initial hardening due to precipitates of metastable γ'' phase and subsequent hardening due to appearance of β .

3. Reduction of FeO by CO

Nearly all processes taking place at a definite rate, and chemical reactions in particular, are associated with an energy of activation representing the minimum energy of the system must acquire before it can undergo the appropriate change (8).

3.1 Potential-energy curves and the Activated State

Consider a reaction involving the atom X and the molecule YZ, viz.,

$$X + YZ = XY + Z$$

The atoms Y and Z in YZ are joined by a single bond, i.e., by a pair of electrons with opposite spins, the atom X is supposed to have an uncoupled electron. As X is brought up to YZ, the interactions of the three electrons causes a decrease in the exchange energy, with the results that the attraction between

Y and Z is diminished and the atoms will tend to separate. The continued approach of X to YZ is thus accompanied by an increase in the potential energy of the system due to the increasing repulsion of X by YZ and the decreasing attraction of Y and Z. Finally, a points is reached at which the atom Z commences to be repelled and the system attains the condition in which the reaction X + YZ = XY + Z can take place. If X is brought still closer to Y, so that the distance between them becomes the normal inter atomic separation, the atom Z is repelled, and the potential energy of the system decreases. The variation of potential energy during the course of the change may be represented qualitatively by moving from left to right along a curve such as is shown in fig. (7). It is evident that before the system X + YZ can become XY + Z i.e., before the reaction under consideration can occur, the reactants must acquire the energy represented by the maximum of the curve. This conclusion may be stated in the figurative form that the reacting system must 'Surmount an energy barrier'. The difference in energy between the initial state and the maximum of the curve, (v) the top of the barrier, is then the energy of activation (E) of the process. The configurates of X-Y-Z at the maximum is called the "activated state" or "activated complex" of the reaction, in this condition the atoms are so disposed with reference to one another that Y can become

associated either with X or with Z, and a very slight displacement will result either in reaction to form XY and Z or in return to the initial state (8).

3.2 CONSTRUCTION OF POTENTIAL-ENERGY SURFACES SEMI-EMPRICAL METHOD

The representation of the variation of the potential energy with inter atomic distance now requires a 3 dimensional model. In order to realize the most favourable conditions for the reaction, however it is necessary that X should approach YZ along the line of centers i.e., X, Y and Z should lie on a straight line (8). By use of the methods and on the assumption that the coulombic energy is a constant fraction of the total energy, for various interatomic distances, obtained from the appropriate Morse equation which gives the dependence of the binding energy E of a diatomic molecule on the distance r between the atoms, with reference to the energy of the separated atoms as zero, it is (9).

$$E = D\ e^{-2\alpha(r-r_e)} - 2e^{-\alpha(r - r_e)}$$

where D is the heat of dissociation of the molecules plus the zero point energy, r_e is the equilibrium inter atomic distance of the normal molecule and α is $0.1227\ w_o\ (\frac{\mu}{D})^{\frac{1}{2}}$, the quantity w_o being the equilibrium vibration frequency and μ, the reduced mass of the molecule. In general, both D' and w_o as well as r_e

are obtained from spectroscopic measurements, since these are known, it is possible to calculate the energy of the diatomic system for any separation of the two atoms.

The potential energy of the system is calculated for a series of values of r_1 and r_2. The results are then plotted on a contour diagram with r_1, i.e., the X-Y distance, as a abscissa and r_2, i.e., the Y-Z distance as ordinate, the various contour lines passing through points of equal energy fig. (8).

It is seen to consist of two valleys, each parallel one of the axes, separated by a pass shaped somewhat like a saddle. At the top of the pass, called the "Saddle point", there is sometimes a shallow basin with gaps leading to the respective valleys. A section through the diagram llel to the r_1 axis at large values of r_2 gives the normal potential-energy curve for the diatomic molecule X-Y; a similar section llel to the r_2 axis will show the dependence of the potential energy of YZ on the atomic separation Y-Z.

The lower right hand portion of fig. (8) represents the energy of the reactants, since Y and Z are then at their normal distances, apart but X is for away from Y, i.e., r_2 is small and r_1 large.

X ---r_1--- Y ---------r_2--------- Z

The final state, with r_1 small and r_2 large, i.e.,

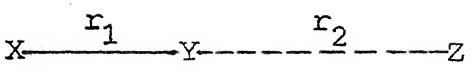

is thus seen to be the top left-hand corner of the diagram.

It is evident that with course of the reaction .. $X + YZ = XY + Z$, the system must pass from the lower right-hand corner to the upper left-hand one of the potential energy surface. The path required by the least energy is indicated by the broken line; the system passes up the bottom of the "horizontal", or "east-to-west", valley, through the gap at the top of the pass, in to the shallow basin, then out of the basin at the other gap and finally down the "vertical", or "north-to-south", valley. By following the reaction path, (i.e.) the broken line, in fig. (8), it is possible to obtain an indication of the relative positions of the three atoms during the course of the reaction. As X is brought upto YZ, the distance between Y and Z is seen to be hardly affected at first, but as X comes closer, the atoms Y and Z begin to be forced apart as a consequence of the repulsive forces between X and Z, which now becomes appreciable when the activated state is reached, at the top of the energy pass, the distance between X and Y is comparable with that between Y and Z, so that Y will be in a position to attach itself either to X or to Z. If it combines with Z, then reaction occurs. If the profile the path were drawn in one plane, it would look someother like that in fig. (9). The classical energy of activation of the process

would be represented by the height of the top of the pass above the level of the ~~metal + metals.~~ initial state.

4. CONCLUDING REMARKS

4.1 A computer model is being analysed using the datas obtained by resistrometric analysis to gain information regarding the nucleation and growth constants during the transformations at different temperatures. The results obtained from hardness measurement with ageing time and the micrographs obtained using Transmission Electron Microscopy will be correlated to the resistivity results.

4.2 The reduction of FeO (solid) by CO (gas) is being considered here. An empirical intermolecular potential function of the form of Morse potential function is used to calculate the activation energy of the activated complex formed during the transformations of reactants to productants using the principles of potential energy surfaces.

The potential energy surface plots gives the least activation energy path for the reduction reaction to proceed and the activation energy for the reduction reaction could be recalculated using the Morse potential functions leading to the understanding of the atomic mechanism of the reduction reaction. A computer model based on bisection-method to determine the roots of the non-linear equation is used to determine and plot the potential energy surfaces of the reduction reaction.

CHAPTER 3

EXPERIMENTAL PROCEDURE FOR RESISTOMETRIC STUDY OF PRECIPITATION IN Ni-Co-Cr-Nb-V SUPERALLOY

3.1 MATERIAL

In the present investigation a nickel-base alloy has been studied, using the methods of electrical resistivity measurements. The Ni-Co-Cr-Nb-V alloy, referred to as nickel-base superalloy has the chemical composition given in the Table III-1.

Table III-1 Chemical composition of the alloy in wt%

Ni	Co	Cr	Nb	V
34.9	34.9	14.2	8.0	8.0

3.2 PROCESSING OF MATERIAL

Before any measurements or observation was made the specimen was subjected to the necessary thermal treatments. All heat treatments were carried out in a tubular, vertical, electrically heated air furnace. The furnace was so designed that with the sample in, it could be closed both from top and bottom. The temperature of the furnace was maintained at the required level and controlled to an accuracy of $\pm$ 2°C by using an Electromax signalling temperature controller. Before every

heat treatment the temperature inside the furnace at the maximum temperature zone was checked and confirmed using a Chromel-Alumul thermocouple and Leeds & Northrup millivolt potentiometer. Pb baths were used for all temperatures measurements till the 100hours of ageing treatments. This provided very less temperature fluctuations during the OFF/ON cycle of the controller of the furnace.

At all stages of heat treatments the specimen was encapsuled in a quartz tube with vacuum of the order of 10^{-3} mm Hg. Also some reactive material like titanium chips were introduced in the quartz tube but carefully protected not to have contact with the specimen at all and to react with any oxygen present.

The solution-treating of the specimen was carried out in a horizontal furnace. At the end of heat treatment the sample was quenched by dropping the encapsled quartz tube containing the sample directly into water bath. In all cases after each heat treatment the specimen was quenched in water. The following ageing temperature and ageing time were studied.

Ageing temperatures in °C : 600°C, 625°C, 650°C, 750°C, 850°C.

Ageing time : 10 minutes to 100 hours

3.3 ELECTRICAL RESISTIVITY MEASUREMENTS

3.3.1 SAMPLE PREPARATION

A piece of (0.254 x 3.07 mm) was carefully cut from the rolled 0.254 mm thick strip, using a mechanical shear. Edges of the cut piece were made smooth and parallel by hand filing using a set of jeweller's needle files. The parallality between the edges were maintained to an accuracy within.

Immediately before the measurement of resistivity the specimen was polished using fine emery paper (4/0 grade). This was done to remove any oxide layer that might have formed on the surface. The polished specimen was washed throughly and wiped dry.

EXPERIMENTAL SET UP

Figure (10) shows the schematic diagram of the set up made use of for measuring the resistivity of the sample. The specimen holder used was made as per the four probe technique. The specimen in the form of a narrow strip was held in the specimen holder by pressing it near the ends against a flat teflon piece by a pair of screws. The potential leads making contact with the specimen at a certain length passed through the screws end were insulated by concentric teflon tubes. The potential leads were spring loaded to ensure proper contact with the specimen. The screws were slidable on the flat teflon piece so that the

length of the specimen at which the potential leads were in contact could be altered. A constant current was made to pass through the specimen by connecting it using the current leads of the specimen holder through the switch SI to a DC constant Source (Model No. HEWLETT 6186).

The resulting potential drop across a certain length AB of the specimen was measured using the L&N K4 potentiometer. The potential leads of the specimen holder connected the specimen to the K-4 potentiometer through the switches S2 and S3. Standard resistance of 10 Ω was induced in the circuit in series with the specimen, so that the same current passed through the specimen and the 10Ω resistance. By the proper positioning of the switches S1, S2 and S3 it was possible to measure the potential drop across either the standard resistance or the specimen in direct or reverse polarity. The unknown e.m.f. (viz) the potential drop across the standard resistance or the specimen was measured by adjusting the potentiometer e.m.f. until an external detector indicated that the potentiometer e.m.f. was equal to the unknown e.m.f. external detector used in the present study was Null detector (Model 7554 K-4) Microvoltmeter. Power supply to potentiometer was provided by constant voltage source of 2V. The set up was designed to ensure that the effect of noise pickup and thermal e.m.f. or the measured value was kept to a minimum. All the resistivity measurements were made

by immersing the specimen in a constant temperature bath maintained between 0°C to 1°C. Normal Hexane was used as the bath medium because of the following reasons: it is not a conductor, does not absorb appreciable moisture, does not react with specimen and remains fluid at 0°C.

3.3.3 MEASUREMENT TECHNIQUES

The polished specimen was fixed in the specimen holder taking care to ensure that the potential and current leads were making proper contacts with the specimen. The holder was then placed in a small rectangular aluminium container filled with normal Hexane to a level well above the specimen. The aluminium container was then placed in an insulated box and was surrounded with crushed ice. The constant current source was switched on and the current adjusted to about 50 mA. Sufficient time (normally about 20 minutes) was allowed so that the current was stabilized and the bath temperature remained stable at 0 to 1°C. Before making any measurement the potentiometer voltage was standardized for the current setting for a reference voltage that is used for comparison with the standard cell voltage. After standardization the switches S1, S2, S3 were so positioned that the voltage drop across the standard resistance could be measured by the potentiometer. The potential drop was measured with direct and reverse current and the mean value obtained. The measured average potential drop across the

standard resistance divided by 10 Ω gave the specimen ($I_{average}$). By this method the value of current was determined to an accuracy of 0.5 μA. In a similar way the average potential drop ($V_{average}$) across the specimen was measured by proper setting of the switches S1, S2 and S3. The length of specimen across wheel the potential drop was obtained was measured by a vernier calliper. A second set of reading for specimen current and voltage were obtained by altering the length of the specimen by sliding the screw containing the potential leads. The average width and thickness of the specimen were measured carefully by a micrometer. The resistivity of the sample for any one length was calculated using the formulae.

$$= R \cdot \frac{A}{l}$$

$$= \frac{V_{average}}{I_{average}} \times \frac{b \times t}{l}$$

where

R = resistivity (Ω cm.)

$V_{average}$ = average specimen voltage (V)

$I_{average}$ = average specimen current (A)

b = average width of the specimen (cm)

t = average thickness of the specimen (cm)
(bst are average of 20 readings each)

l = length of the specimen across which the potential drop in measured (cm)

The resistivity of the sample was computed as the average of the two sets of values measured for two different lengths.

Chapter -4

RESULTS AND DISCUSSION OF PRECIPITATION KINETICS IN THE NICKEL - BASE ALLOY

4.1 Variation of Resistivity with time

The sample of Ni - base superalloy was solution treated and aged at 600, 625, 650, 750 and 850°C for various lengths of time and the resistivity was measured. The same sample was used for all measurements and a freshly solution treated sample was used for each temperatures. The Resistivity of the solution treated sample is listed in table [1] along with its history. Small scatter in the values of the resistivity of the solution treated samples show dissolution of precipitates if any, complete homogenization and reproducibility of the technique used. The difference between resistivites of solution treated samples are sometimes large. However further evaluation requires $\Delta\rho$. Therefore the differences are not important.

The Resistivities of aged samples were subtracted from that of the homogenized sample. The resulting $\Delta\rho$ values have been plotted in figures [10a], [10b] and tabulated in table [2]. It is clearly seen that at 600, 625 and 650°C the resistivity shows continuous increase on Ageing, reaches a maximum and decreases. This Kinetic behaviour is same at the three

temperatures 600, 625 and 650°C. The other two ageing curves corresponding to 750°C and 850°C are distinctly different in their behaviour. Although the 850°C curve shows the typical increase in Resistivity with Ageing time, attainment of maximum and decrease in Resistivity, the curve at 750°C shows hardly any increase in resistivity with increase in Ageing time. This difference in behaviour between the two sets of curves clearly suggest that the precipitating phase might be different in the two different temperature ranges.

4.2 Precipitate Sequence in the Ni - base alloy

The precipitate sequence in the Ni - base alloy used in this investigation has been investigated by TEM by JENA and CHATURVEDI. They have shown that at 650°C Primary γ'' precipitate as shown in fig.[2] and fig.[6]. These two figures clearly show procipitates of γ''. This was confirmed by suitable Electron diffraction pattern. Their investigation of the alloy aged at 750°C shows a mixture of both γ'' and β as shown in fig.[10c] and fig.[10d] which is a dark dield micrograph showing white r'' procipitates and long rod like precipitates. This work clearly shows that at 650°C one phase γ'' appears in the early stage and at 750°C the two phases β and γ'' form simultaneously. At 850°C the alloy contains primarily β precipitate and a very few γ'' precipitates as shown in fig.[10e]. Fig.[10e] shows stacking faults, needles of β and very fine

precipitates of γ'' in the matrix. These are detectable only by weak diffraction patterns.

This is also confirmed by the Hardness vs Ageing curve shown in fig.[1].

The Resistivity plot for 600°C, 625°C and 650°C are due to precipitation of single phase γ''. The Resistivity plots at 750°C is due to simultaneous precipitations of both γ'' and β. The Resistivity plot at 850°C is essentially due to formation of β.

4.3 Kinetics of precipitation

Precipitation Kinetics in this case is followed by Recording the resistivities of the alloy. The total resistivity of the alloy may be expressed by the following expression.

$$\rho = \rho_m V_m + \rho_p V_p + \rho'_s (n, v) \qquad (1)$$

where

ρ = resistivity of the aged sample

ρ_m = resistivity of the matrix at any instant

V_m = volume fraction of the matrix

ρ_p = resistivity of the precipitate which is a function of its compusition and hence time

V_p = volume fraction of the precipitate

ρ'_s = contribution to the resistivity due to the strain associated with the precipitation

n = number of precipitate particles

v = average volume of the precipitate particles

It is reasonable to assume that $V_m \simeq 1$ and V_p to be very small. Also in the highly super saturated solid solution most of the precipitation nucleate in very early stage at a high nucleation rate. Therefore the number of nuclei, like those of γ'' may not change appreciably with time. Since the average radius of the precipitate is proportional to $t^{1/3}$ which is the common coarsening behaviour of such particles, the volume of the precipitate is taken as proportional to t and hence the above equatation reduces to the following

$$\rho = \rho_m + \rho_s \cdot t \qquad (2)$$

where ρ_s is a measure of contribution of the strain energy of precipilate to the resistivity.

Therefore the expression for $\Delta\rho$ is as follows

$$\Delta\rho = \rho - \rho_m(t = 0) = \rho_m - \rho_m(t = 0) + \rho_s \cdot t$$

or $$\Delta\rho = \Delta\rho_m + \rho_s \cdot t \qquad (3)$$

$\Delta\rho_m$ is expected to decrease with time and approach a constant value whereas ($\rho_s \cdot t$) will change linearly with time. Two situations may be visualized as shown in fig.[a, b]

If for a precipitation ρ_s is very large the situation becomes similar to that shown in fig.(a) whereas if ρ_s due to precipitation is less the situation would be that shown in fig.(b).

The strain energy associated with formation of β is much less as it is partially coherent. Examination of the vs t curve for 850°C is similar to that shown in fig.(b). On the other hand the strain due to formation of γ'' is much higher and the $\Delta\rho$ vs t curve at 600, 625 and 650°C are as expected similar to that shown in fig.(a).

It is noticed that at 750°C below 30 minutes the $\Delta\rho$ vs t curve corresponds to the precipitation of γ'' whereas that above 40 minutes corresponds to the precipitation of β suggesting that at 750°C sudden appreciable precipitation of β must have taken place after 30 minutes of Ageing. This is borne out by the Hardness vs Ageing time curve at 750°C shown in fig.[1].

The $\Delta\rho$ vs t plots at 600,625 and 650°C show that the peak resistivity at the higher temperature of 650°C appears at higher ageing time. The magnitude of $\Delta\rho$ is also higher compared with that at 600°C. This is inconsistent with precipitation of a single phase γ''. However if precipitation of β occurs at 650°C slowly after 300 minutes the resistivity would continue to increase. It has been clearly shown by the Micrographs of JENA and CHATURVEDI that needles of β are observable at 650°C after about 300 minutes.

4.4 A Kinetic model

White et al (10) in their investigation of Ageing in Nimonic alloys have proposed a model for calculating the resistivities. In this model, the impurity population was divided in to three groups, namely impurities in solution, impurities in small clusters and impurities in large clusters. It is assumed nucleation occurs due to the movement of solute in the matrix, n_i, to the small clusters containing n_s number of solute atoms. The growth process involves movement of solutes from group n_s to n_l where n_l represents large cluster or precipitates. Thus the total resistivity is expressed by following equation:-

$$\rho = \rho_{matrix(pure)} + \rho_i X_i + \rho_s X_s + \rho_l X_l \qquad (4)$$

Where ρ_{matrix} represents the resistivity of the solute free mattrix. ρ_i, ρ_s, ρ_l represents resistivity contributions from the solutes in their respective groups and X_i, X_s and X_l represent fraction of solutes in their respective groups. Assuming first order Kinetics and taking total number of solutes to be n_o it can be shown that,

$$\frac{n_i}{n_o} = \exp(-K_1 t) \qquad (5)$$

$$\frac{n_s}{n_o} = \frac{K_1}{K_2 - K_1}\left[\exp(-K_1 t) - \exp(-K_2 . t)\right] \qquad (6)$$

$$\frac{n_l}{n_o} = \left[1 + \frac{K_1 \exp(-K_2 . t) - K_2 \exp(-K_1 . t)}{K_2 - K_1}\right] \qquad (7)$$

Hence the equation reduces to:-

$$\rho = \rho_{matrix} + \rho_i\left(\frac{n_i}{n_o}\right) + \rho_s\left(\frac{n_s}{n_o}\right) + \rho_1\left(\frac{n_1}{n_o}\right) \qquad (8)$$

This equation contains two rate constants K_1 and K_2 and four other constants ρ_{matrix}, ρ_i, ρ_s and ρ_1. These constants were evaluated such that the experimental ρ Vs ageing time curve could be reproduced. They have obtained reasonable values for these constants and reasonable activation energies which are of the order of 1.11 to 1.83 eV.

This model was also tried out for the present system. The expression for the ρ of Aged samples were taken from the tables and the Dec 10 computer of the Institute was used to evaluate the constants using the Least square fitting technique The program is attatched in Appendix (A).

The results obtained from the analysis are listed in Table [3]. It may benoted from the table, the constant ρ_{matrix} obtained in this investigation matches well with those reported by White etal. Values of ρ_i are also of the same order. Some of the values of ρ_i is - ve and this is highly improbable. ρ_s values obtained in this investigation are large and positive which is to be expected. However the magnitudes are much higher than those of White etal. Negative values for ρ_1 has been obtained from the present data. This is not improbable. However the values reported by White etal were positive. The values of rate constants

K_1 matches very well with these reported by White etal where as rate constant K_2 agrees reasonably well at 600°C but differ appreciably at 650°C. The temperature dependence of K_1 shows the right trend as the values of K_1 at 650°C is higher than that at 600°C.

The poor applicablity of the model proposed by White etal to the present alloy may be attributed to the nature of the alloy. In the present investigation γ'' precipitated, this phase is associated with very high strains because of Large mismatch with the matrix compared with γ' which precipitated in the alloy used by White etal. This is reflected in the maximum change in the resistivity of the alloy at about 650°C, White etal. obtained a change of about 1% whereas in this investigation the change in the same temperature was 6 times greater. The high strain associated with γ'' precipitation makes the contribution of the precipitates to resistivity rather complex as it has been pointed out in the previous section. Therefore the simplistic model proposed by White etal which was satisfactory for precipitation of γ' is not applicable to the present system containing precipitates of γ''.

CHAPTER 5

ATOMIC MECHANISM OF REACTIONS INVOLVED IN REDUCTION OF FeO BY CO

5.1 General

A great majority of the work on reaction rates now being done is primarily concerned with tyring to find out exactly in what manner the reaction are proceeding. Kinetic study provide an insight of determining the mechanism of reaction. A possible mechanism of the following reduction reaction is studied.

$$FeO\ (solid) + CO\ (gas) \quad CO_2\ (gas) + Fe\ (solid)$$

5.2 A Physical Model

FeO has NaCl structure (Fig. 13), considering interaction of CO molecule with the (010) surface of FeO crystal. On the surface each oxygen atom has six Fe-atoms as neighbours. So there are only Fe-O interaction. The reaction can be considered as follows. (Fig(12a))

Step 1 CO molecule is far away from the (100) surface of FeO

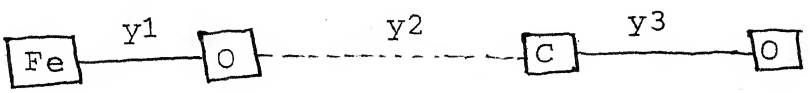

where

y1 = a distance parameter representing interaction between Fe atoms and O atoms in FeO lattice.

- Fe atom

O - Oxygen atom

Fig. 12a FeO unit cell

y2 = symbolizes zero interaction between FeO lattice and CO molecule. Here in step 1 y2 = ∞

y3 = a distance parameter representing interactions between C atom and O atoms in CO molecule.

Step 1 symbolizes the interaction at time (t = 0. It is the initial state.

Step 2 Fig. 12b

Step 2 symbolizes that there is now some interaction of FeO lattice with CO molecule as the interaction distance between the two which is denoted by $y2 = \infty$ in the initial state has now changed to some defined interaction distance parameter.

Step 3

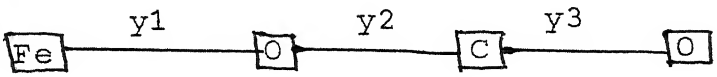

Step 3 symbolizes appreciable interaction.

Step 4

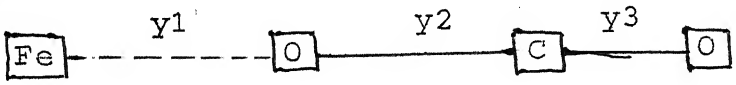

At time (t) = t final

$y1 = \infty$, $y2 = y3$ = a distance parameter representing interaction in CO_2 molecule represented by Y_o.

At $t = 0$ (initial state)

$y1 = y1_{Fe-O}$

$y2 = \infty$

$y3 = y3_{C-O}$

At $t = t$ final (final state)

$y1 = \infty$

$y2 = y3 = Y_o\ CO_2$

E = Energy of formation (Bond energy)

$\therefore E = f(y1, y2, y3)$

5.3 CHANGE OF ENERGY OF THIS 3YSTEM

5.3.1 BONDING BETWEEN TWO ATOMS

The function which it is proposed to use here is the Morse potential.

The atoms of a molecule are acted on by two types of forces, fundamentally electrical in origin. First, there are forces of attraction, the force which are concerned in chemical binding, often called valence force. These forces fall off rapidly as the distance r between the atoms increases, increases rapidly with decreasing r. Being attractive they are negative forces (curve I). (Fig. 13)

Secondly, there are repulsive forces, quite negligible at large distance, but increasing even more rapidly than the attraction at small distances. The repulsion, a force of the sign is shown in (curve II). (Fig. 13)

Fig. 13

5.4 MORSE POTENTIAL

Assuming F to be exponential let

$$F = Ae^{Br} \tag{1}$$

At equilibrium $|F_{rep}| = |F_{attractive}| = F^*$

and $r = r_e$ (2)

$\therefore\ F^* = Ae^{Bre}$

or $A = F^* e^{-Bre}$

$F = F^* e^{-Bre} \cdot e^{Br}$

$F = F^* e^{B(r-re)}$

when $r > r_e$, F must decrease. Therefore it is $e^{-B(r-r_e)}$ and when $r < r_e$, F increases.

Hence

$$F = F^* e^{-B(r-r_e)} \tag{3}$$

Let $F^* = 2D\alpha$

$B = 2\alpha$

The general repulsive force

$$F = 2D\alpha e^{-2\alpha(r - r_e)} \tag{4}$$

where D, α are constants

r = interatomic separation between two atoms

re = equilibrium separation between the two atoms

Similarly attractive force

$$F = - A' e^{B'r}$$

at $r = r_e$ $\quad F^* = - A' e^{B're}$

$$F = - F^* e^{B'(r-re)}$$

Let $B' = \frac{B}{2} = \frac{2\alpha}{2} = \alpha$

when $r > r_e$ $\quad |F|$ must decrease

$$F = - F^* e^{-B'(r-re)}$$

The general attractive force

$$F = - 2 D\alpha e^{-\alpha(r-re)} \qquad (5)$$

$\therefore$ Repulsive force $F = 2D\alpha e^{-2\alpha (r-re)}$

Attractive force $T = - 2D\alpha e^{-\alpha(r-re)}$

where D, α are constants.

$$F_{Net} = F_{repulsive} + F_{Attractive}$$

$$F_{Net} = 2D\alpha e^{-2\alpha (r-re)} - 2D\alpha e^{-\alpha(r-re)}$$

when $r = re$, $F_{Net} = 0$

At the distance re, where the forces changes sign there is a position of equilibrium. The attraction and repulsion just balance and the atom can remain at that distance apart indefinitely. This is the normal distance of separation of the atoms in the molecules.

ENERGY

For a diatomic molecule in a physically stable state, the potential energy must have a minimum when the separation between the two atomic nuclei has its equilibrium value, which is determined by the balance between the attractive force due to the electronic binding and the columbic repulsion between the charged nuclei. If the atoms are brought closer than this equilibrium separation, then the potential energy must rise sharply due to the work done against the increasing repulsive force between the nuclei. If the atoms are drawn apart, thus the potential energy must also rise due to work against the now superior electronic binding force, as the separation between the atoms increases the potential energy must approach a limiting value which will be the dissociation energy of the molecule. This simple physical picture of the molecular system leads to a potential curve with a minimum at the equilibrium internuclear distance, a sharp rise towards infinty as the nuclei

Fig. 14

are brought together, and a less sharp rise towards the dissociation limit as the separation is increased. (Fig·14)

Assumption : Separation at ∞ , E = 0

Increase in energy of the system due to repulsion. (Try to move from r to r = ∞ the energy spent is given by

$$= - \int_{r}^{\infty} 2D \propto e^{-2\propto (r-re)} \, dr$$

$$= \frac{-2D\propto}{-2\propto} \left[e^{-2\propto (r-re)} \right]_{r}^{\infty}$$

$$= + D \, e^{-2\propto (r-re)}$$

Increase in energy of the system due to attraction (Try to move from r to r = ∞ the energy spent is

$$= - \int_{\gamma}^{\infty} - 2 \, D\propto e^{- \propto (r-re)} \, dr$$

$$= \frac{\pm 2D\propto}{-\propto} \left[e^{-\propto (r-re)} \right]_{\gamma}^{\infty}$$

$$= - 2D \, e^{-\propto (r-re)}$$

$$E_{Net} = E_{Repulsive} + E_{Attractive}$$

$$E = + D \, e^{-2\propto (r-re)} - 2De^{-\propto (r-re)} \qquad (6)$$

Er = re = D-2D = - D where D = Dissociation energy

This function has a minimum of -D at r = re, comes asymptotically to zone at r = ∞ . The only portion where it does not fit is at r = o where it should be infinity. But for the

values of D and α, E(r) is between 100D and 10,000 D at r = re, a value so large that, as for as its effect on the energy levels and wave functions goes, it is as good as infinity.

5.5 PHYSICAL SIGNIFICANCE OF α

$$F = 2\alpha D \left[e^{-2\alpha(r-re)} - e^{-\alpha(r-re)} \right]$$

using Taylor's expansion in (r-re) for small displacements.

$$F = 2\alpha D \left[1 - 2\alpha(r-re) \ldots\ldots - 1 + \alpha(r-re) \right]$$

$$F = -2\alpha^2 D (r-re)$$

Here Force $\propto$ K (r-re)

where $K = 2\alpha^2 D$ = a constant

$\therefore$ α is related to force constant

$$E = De^{-2\alpha(r-re)} - 2De^{-\alpha(r-re)}$$

$$\frac{\partial E}{\partial r} = -2D\alpha e^{-2\alpha(r-re)} + 2De^{-\alpha(r-re)}$$

$$\left(\frac{\partial E}{\partial r}\right)_{r=re} = 0 \quad \text{here E is minimum}$$

$$\left(\frac{\partial^2 E}{\partial r^2}\right) = 4D\alpha^2 e^{-2\alpha(r-re)} - 2D\alpha^2 e^{-\alpha(r-re)}$$

$$\left(\frac{\partial^2 E}{\partial r^2}\right)_{r=re} = 2\alpha^2 D$$

$\therefore$ $\left(\frac{\partial^2 E}{\partial r^2}\right) > 0$, E is minimum at r = re

$$\text{curvature} = \frac{1}{\text{Radius of curvature}}$$

$$= \frac{d^2y/dx^2}{\left[1 + \left(\frac{dy}{dx}\right)^2\right]^{3/2}}$$

$$= \frac{2\,D\,\alpha^2}{\left[1 + 0\right]^{3/2}}$$

curvature at minimum = $2\,D\alpha^2$

5.6 EQUATION FOR ENERGY OF FORMATION OF CO (DIATOMIC MOLECULE)

$$C\ (g) + O\ (g) \longrightarrow CO\ (g)$$

$$E = De^{-2\alpha(r-re)} - 2D\,e^{-\alpha(r-re)}$$

This problem requires that a computer program be written to calculate the energy of formation of CO

5.6.1 The input data include

D = Dissociation energy of CO in kcal/mole

$$O(g) + C(g) \longrightarrow CO(g)$$

$$C(s) + \tfrac{1}{2}\,O_2(g) \rightleftharpoons CO(g) \quad \Delta H_o^o \ (I)$$

$$\tfrac{1}{2}\,O_2 \rightleftharpoons O\ (g) \quad \Delta H_o^o \ (II)$$

$$C(s) \rightleftharpoons C(g) \quad \Delta H_o^o \ (III)$$

$$C(g) + O(g) \rightleftharpoons CO(Co)$$

$$\Delta H_o^o = \Delta H_o^o\ (I) + \Delta H_o^o\ (II) - \Delta H_o^o\ (III)$$

$$= -\ 255.764 \text{ kcal/mole}$$

The equation above was evaluated using the computational facility. The program is listed in Appendix (B). The values of E in KCal obtained from this program have been plotted against inter atomic distance γ in Fig [15]. The shape of the curve, as expected is satisfactory and suggests that the Morse potential could be used to calculate energy of interaction between the atoms.

5.6. Energy of formation of CO_2

The energy of formation of CO_2 can be modelled in the following manner. Firstly, the interaction between one O atom and the Carbon atom may be considered ignoring the presence of the second one. The interaction of the C atom and the second O atom would be similar. However because of the presence of two oxygen atoms the energies calculated in the above manner would not be correct and a correction term have to be introduced in order to take care of the influence of the two oxygen atoms. Using the Morse potential equation for the two atoms equation (6) the energy of CO_2 may be written in the following manner. Designating one of the oxygen atoms with a subscript 1 and the other oxygen atom with a subscript 2 we may write the following equation:-

$$E = [\, De^{-2\alpha(\gamma_1 - \gamma e)} - 2De^{-\alpha(\gamma_1 - \gamma e)} \,]_1$$

$$+ [\, De^{-2\alpha(\gamma_2 - \gamma e)} - 2De^{\alpha(\gamma_2 - \gamma e)} \,]_2$$

$$+ Ae^{-B(\gamma_1 + \gamma_2 - 2\gamma e')}$$

Where D is the Dissociation energy of CO

α is same as that for CO

γe is equilibrium distance in CO

$Ae^{-B(\gamma_1 + \gamma_2)}$ = Correction term due to the two oxygen atoms.

γ_1 the distance between oxygen atom designated by 1 and the C atom and γ_2 the distance between oxygen atom designated by 2 and the C atom.

$\gamma_1 + \gamma_2 - 2\gamma e'$ = the distance between oxygen atom in excess of the equilibrium O - O distance in CO_2.

Let $\gamma e'$ be the equilibrium distance between the C and oxygen atoms in CO_2. Hence

$$\gamma_1 - \gamma e = (\gamma_1 - \gamma e') + (\gamma e' - \gamma e)$$

$$\gamma_2 - \gamma e = (\gamma_2 - \gamma e') + (\gamma e' - \gamma e)$$

Let $(\gamma_1 - \gamma e') = R_1$

$(\gamma_2 - \gamma e') = R_2$

$(\gamma e' - \gamma e) = \varepsilon$

hence

$$(\gamma_1 + \gamma_2 - 2\gamma e') = (\gamma_1 - \gamma e') + (\gamma_2 - \gamma e')$$
$$= R_1 + R_2$$

and

$$E = \underbrace{De^{-2\alpha(R_1 + \varepsilon)} - 2De^{-\alpha(R_1 + \varepsilon)}}_{1} + \underbrace{De^{-2\alpha(R_2 + \varepsilon)} - 2De^{-\alpha(R_2 + \varepsilon)}}_{2} + Ae^{-B(R_1 + R_2)}$$

ABL et al (11) have considered the interaction between the O - O atoms and have been also to calculate the constants A and B. Taking their values of A = 171 Kcal, B = 1.086 A^{o-1} and assuming ε = 0.061 A^{o} the atoms equation was evaluated extending R_1 and R_2 up to infinity. The calculation were made using DEC 10 Computer adopting the principles of Bi section Method to determine the roots of the non-linear equation. The program is attatched in Appendix (C).

The potential energy contours due to interaction between C and the two O atoms is shown in Fig. [16]. It is clearly shown that the energy of formation of CO_2 from gaseous O atoms and C is less than - 325 K.Cal. This may be compared with the thermodynamic data calculated in the following manner.

Let.

$$O_2(g) + C(g) \longrightarrow CO_2,\ \Delta H_o^o(I) = -93.96 \text{ Kcal/mole}$$

$$2O \longrightarrow O_2,\ \Delta H_o^o(II) = -117.978 \text{ Kcal/mole}$$

$$C(g) \longrightarrow C(s),\ \Delta H_o^o(III) = -169.580 \text{ Kcal/mole}$$

$$C(g) + (2\,O(g) \longrightarrow CO_2,\ \Delta H_o^o = -381.524 \text{ Kcal/mole}$$

It is seen that the calculated value compares very with the experimental values although the equation does'nt use the dessociation energy of CO_2 anywhere in the calculation. Therefore the agreement is considered to be good.

5-7 Activation energy for the formation of CO_2 from CO and O

If the seperation between C and one of the O atoms is varied from $\gamma e'$ ($\simeq 1.16 A^{\circ}$) to γe ($\simeq 1.13 A^{\circ}$) while the distance between the other oxygen atom and carbon is extended upto infinity one could trace the variation of energy of the system along the reaction path. Since the difference between $\gamma e'$ and γe is too small to be detected in the Fig.(16) of potential energy contours variation of E with R_1 has been ploted in Fig.[17] keeping R_2 fixed at $1.16 A^{\circ}$. The figure clearly shows the system has to go through a maximum in order to reach the equilb. CO_2 configuration. The value of energy of formation of CO_2 turns out to be - 325 Kcal and the activation energy for the formation of CO_2 from O and CO turn out to be 22.0 Kcal. The activation energy turns out to be reasonable as atomic oxygen is involved in the reaction. The presence of an activation barrier is primarily due to repulsion of oxygen atoms.

5.5 Interaction between FeO, CO, CO_2

Consider a model as shown below:

Fe — O — C — O

The interaction energy in this system can be considered as a first approximation to be due to Fe-O, O-C, C-O interactions. Therefore the total energy is given by the following expression:

$$E = \left[D_1 e^{-2\alpha_1(r_1-re1)} - 2D_1 e^{-\alpha_1(r_1-re1)}\right]_{Fe-O} + \left[De^{-2\alpha(r-re)} - 2De^{-\alpha(r-re)}\right]_{O-C} + \left[De^{-2\alpha(r-re)} - 2De^{-\alpha(r-re)}\right]_{C-O} \quad (1)$$

where D_1 , α_1 , r_1, re1 corresponds to the Fe-O bond. The values of D_1 is estimated from the heats of formation of FeO from Fe and O for a single Fe-O bond in the following manner.

$Fe + \frac{1}{2} O_2 \longrightarrow FeO$ $\quad \Delta H_1(298.15) = -63.7$ K Cal/mole

$\frac{1}{2} O_2 \longrightarrow O$ $\quad \Delta H_2(298.15) = +59.1$ K Cal/mole

---

$Fe + O \longrightarrow FeO$ $\quad \Delta H_3 = -122.8$ K Cal/mole

$$\Delta H \text{ of Fe-O bond} = \frac{\Delta H_3}{\frac{1}{2} NZ} = \frac{\Delta H_3}{3N}$$

$$\Delta H/\text{mole of FeO bond} = \frac{\Delta H_3}{3} = -40.9 \text{ K cal/ mole}$$

of FeO was evaluated from the relation (12)

$$\frac{1}{K} = \frac{1}{9C\ N\ a_o}\left(\frac{d^2E}{da^2}\right)_{a = a_o} \qquad (2)$$

where the compressibility K is given by the Gruneisen Relation. This relation is between the three important physical properties (δ, the coefficients of thermal expansion, C_v, the specific heat constant volume and K the compressibility) of a solid. Thus for a solid of volume V_o

$$K = \frac{\delta\ V_o}{C_v \cdot \gamma} \qquad (3)$$

where γ is the Gruneisen constant and $\simeq 2$

N is the total number of atoms in the crystal

C = 4 (B.C.C)( )

$\simeq$ 2 (F.C.C)

a = Lattice parameter

Taking δ = 12 x 10^{-6} /degree

V_o = 12.011368 cm^3

R = 8.314 x 10^7 erg/degree-mole

C_v = 3R = 24.92x10^7 erg/degree-mole

K is calculated as 0.2891974x10^{-12} cm^2/dyne.

From the work of (12) it can be shown that

$$\frac{1}{K} = \frac{1}{9CNa_o}\left\{4\alpha^2 L\beta^2 \sum_j M_j^2 e^{-2\alpha a_o M_j}\right\} - \frac{1}{9CNa_o}$$

$$\left\{2\alpha^2 I\beta \sum_j M_j^2 e^{-\alpha a_o M_j}\right\} \qquad (4)$$

where $r_j = [n_j^2 + l_j^2 + m_j^2]^{\frac{1}{2}}$ $a = m_j a$

Let $L = \frac{1}{2} ND$, $= e^{r_o}$, $(r_j = M_j$ (only for cubic metals)[12]$)$

and $(E = \frac{1}{2} ND \sum_j e^{-2\alpha(r_j - re)} - 2e^{-\alpha(r_j - re)})$ [12]

The equation reduces to

$$\frac{1}{K} = 3.30483 \times 10^{-5} \alpha^2 \left\{2 e^{-4.30\alpha} \; 0.25 e^{-4.30 \times 0.5\alpha} \; e^{-1.0752\alpha}\right\} \qquad (5)$$

where $\frac{1}{K} = 3.45784 \times 10^{-12}$ dynes/A^{o2}

Solving for (5) one finds $\alpha_{Fe-O} = 1.265 A^{o-1}$ and this value of α compares reasonably with value of α of Fe ($= 1.338 A^{o-1}$).

r_{e_1} of FeO is $\simeq$ 2.155 A^o

Making use of the above equation (1) potential energy curves were obtained using a programme listed in Appendix D. Unfortunately the results are not satisfactory. The energy of formation of the complex Fe-O-C-O is found to be very high and negative. This is probably because of the fact that the assumptions were notsufficiently rigorous. For example the C-O

interaction and Fe-C interaction were ignored and C-O interaction was kept constant. Also isolated Fe-O bond was considered rather than a solid crystal of FeO. The results would certainly improve if the above constraints are removed. However consideration of the interation of CO with solid FeO would involve considerably more work which may be taken up as an extension of present work.

SUMMARY AND CONCLUSIONS

1. In order to investigate the precipitation Kinetics in a Ni - CO - Cr - Nb - V superalloy the resistivity of a homogenized alloy was measured. The homogenized sample was aged at 600, 625, 650, 750 and 850°C up to 100 hours and the variation in resistivity was measured. The values for 600, 625, and 650°C show increase with time, attainment of a maximum and decrease on further ageing. The $\Delta\rho$ values at 850°C show first a decrease and then an increase with time and at 750°C $\Delta\rho$ Vs ageing time curve behaves like the low temperature curve up to 30 minutes when it suddenly changes its behaviour to that observed at 850°C.

2. The Resistivity data is consistent with TEM observations represented in literature. At temperatures below 650°C precipitation of γ'' and at temperature of 850°C the precipitation of β are expected to lead to observed shapes of $\Delta\rho$ Vs ageing time plot. The $\Delta\rho$ curve at 750°C suggest sudden onset of β precipitation after about 30 minutes. The temperature dependence of the ageing times at 650°C β phase may be precipitating showly. This is also consistent with the TEM observation.

3. The model proposed by White et al for predicting the resistivity variation in aged superalloys is too simplistic to be applicable to the present system.

4. The second kinetic problem investigation related to the reduction of FeO by CO and CO_2. The potential energy of a system of atoms has been represented by a Morse potential. Suitable constants of the potential have been either taken from the literature or estimated. Using these constants potential energies and potential energy Contours have been calculated using the DEC 10 Computer.

5. The calculated potential energy diagram for CO has the expected shape.

6. The potential energy diagram of CO_2 has been calculated and plotted. The activation energy for the interaction of O with CO has also been estimated to be 22 Kcal. The calculated dissociation energy of + 325.5 Kcal/mole compare very well with values of + 381 Kcal/mole calculated from the thermodynamic data.

7. The potential energy calculations however could not be extended satisfactorily to FeO as some of the critical data's for evaluation of the Morse potential are not yet available. However once the values of the constants are available it will be a simple matter to extend the calculation involving FeO, CO and CO_2.

I.I.T. KANPUR
CENTRAL LIBRARY
Acc. No. A 83735

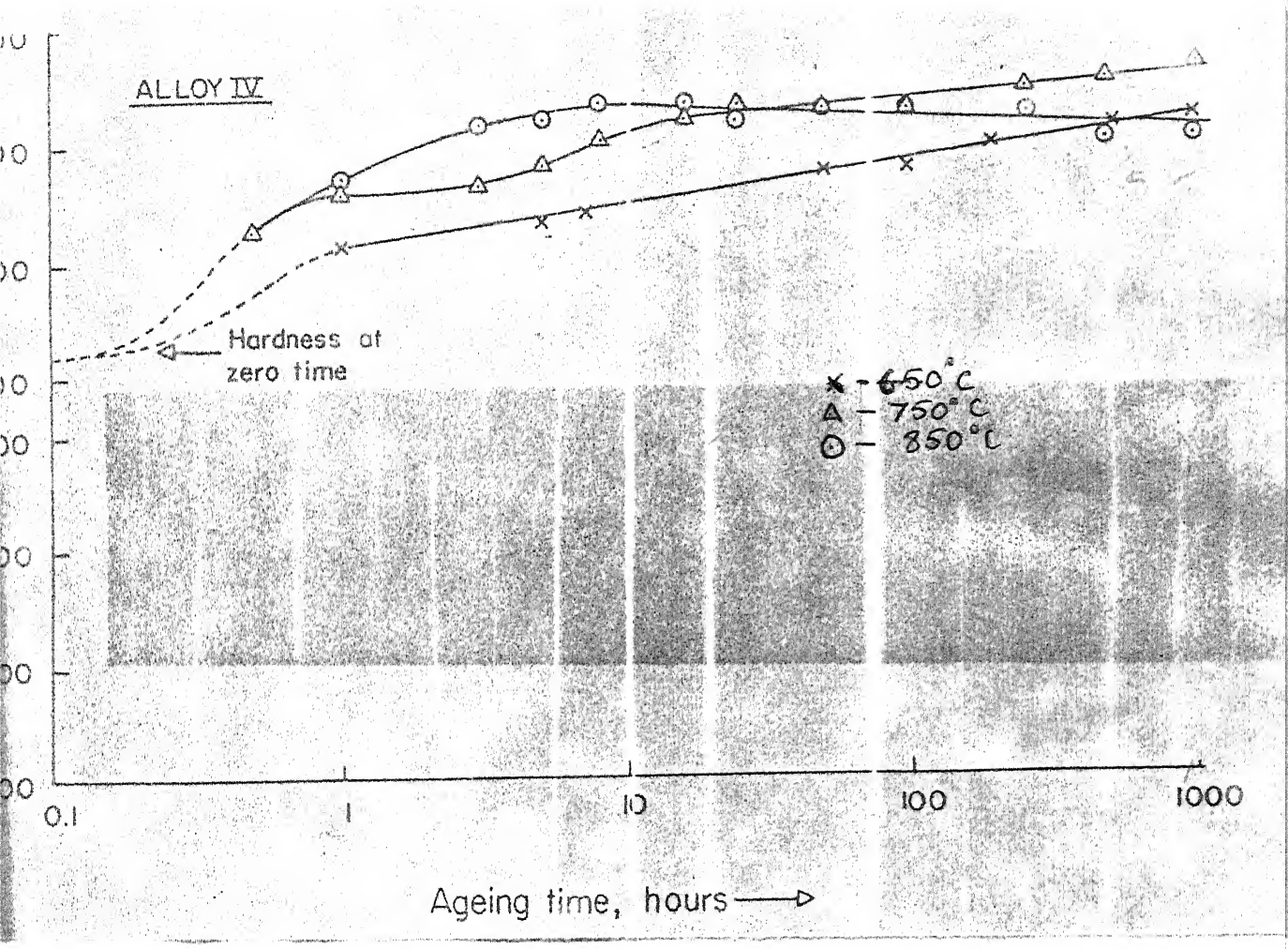

Fig.1 Hardness ageing curves for alloy at 650°c, 750°c, and 850°c

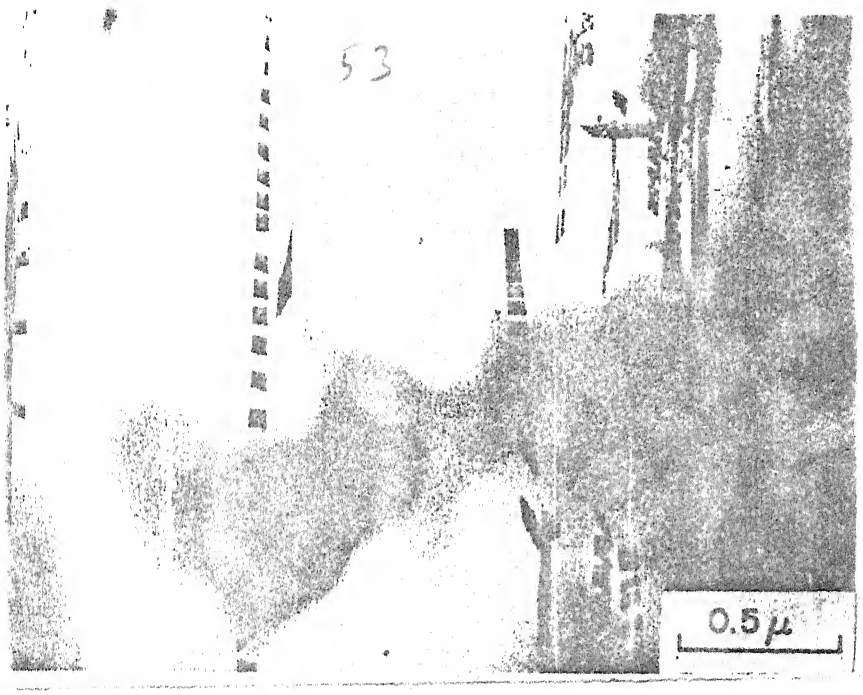

Fig.2 Structure of alloy aged for 1 hour at 650 c

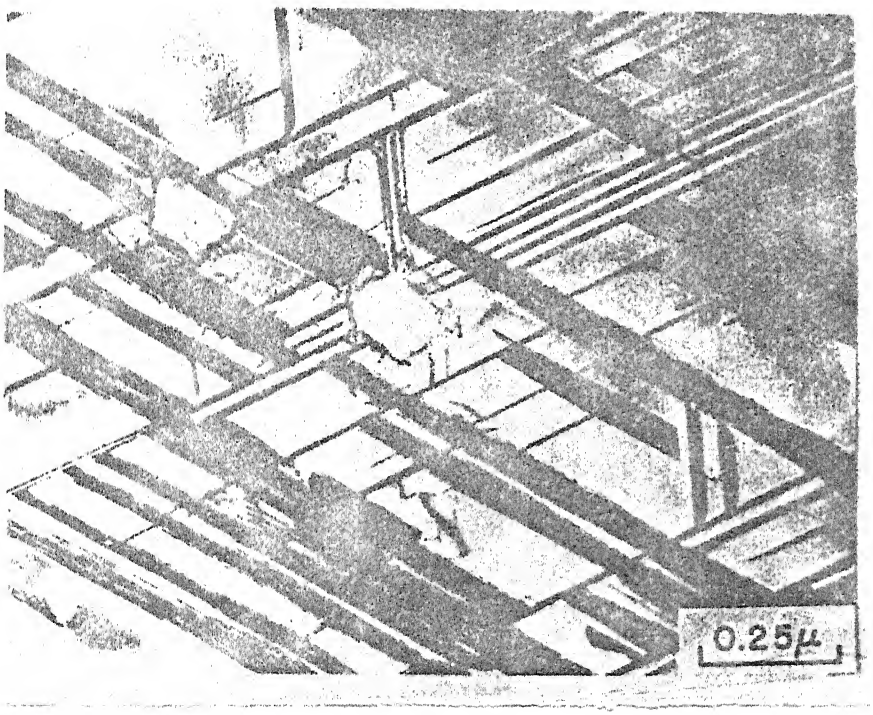

Fig. 3 Structure of alloy aged for 1 hour at 850 c

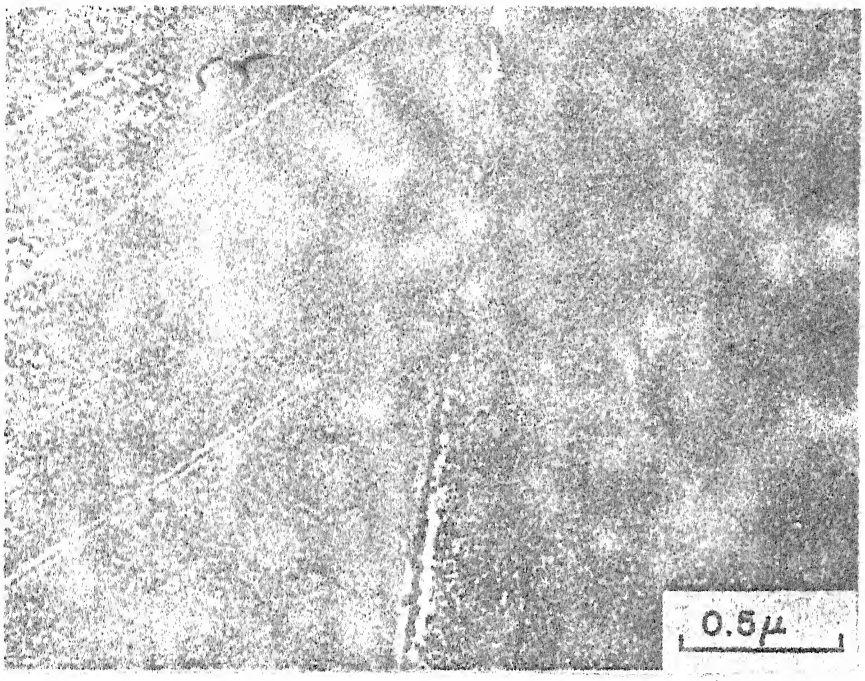

Fig. 4 Structure of alloy aged for 3 hours at 750 c

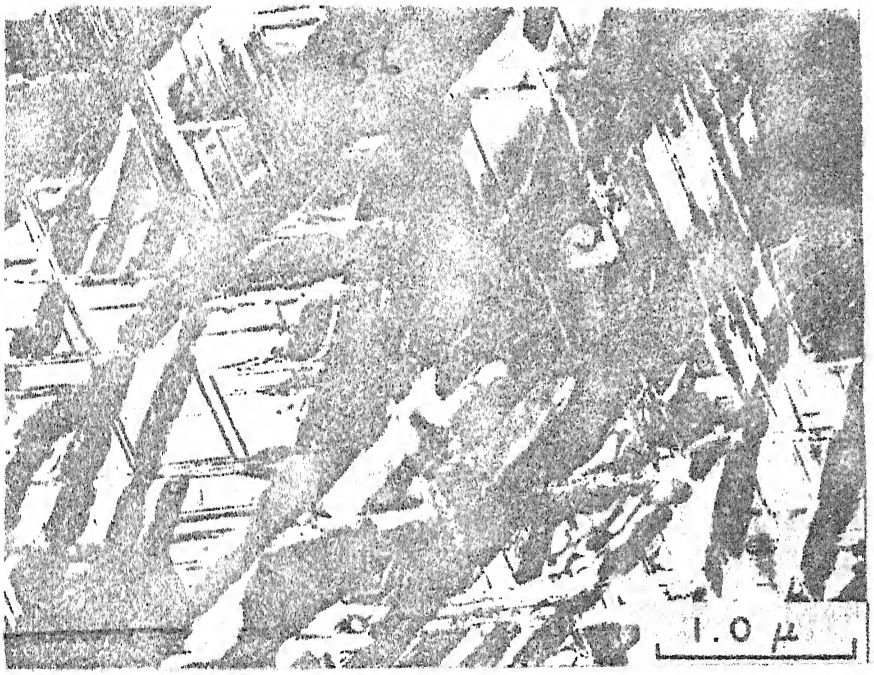

Fig. 5 Structure of alloy aged for 1039 hours at 750 c

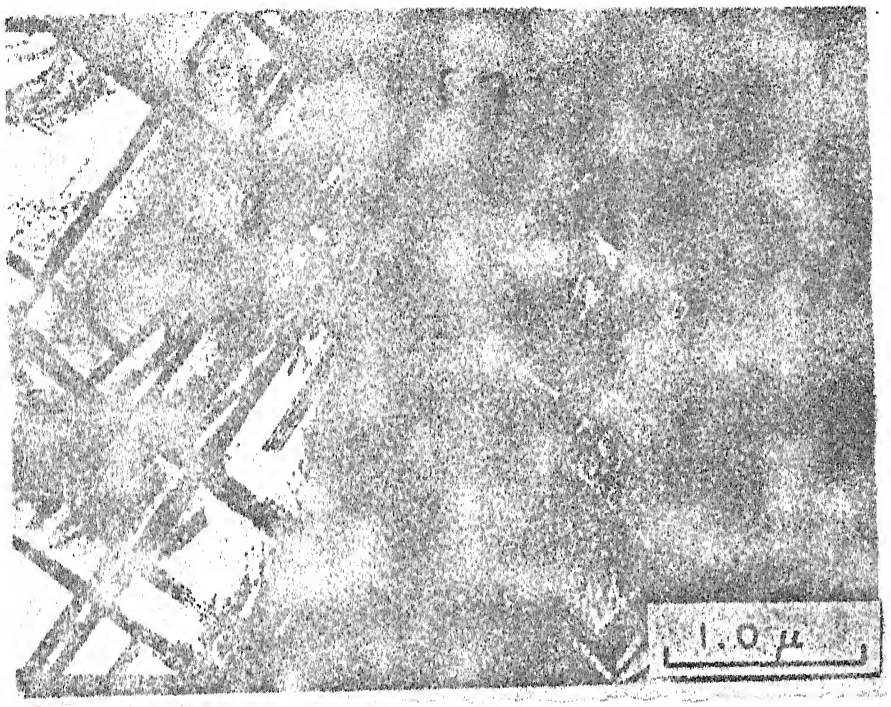

Fig.6 Structure of alloy aged for 1039 hours at 650 c

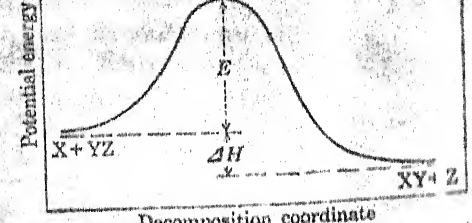

FIG. 7.—Variation of potential energy accompanying the reaction $X + YZ = XY + Z$.

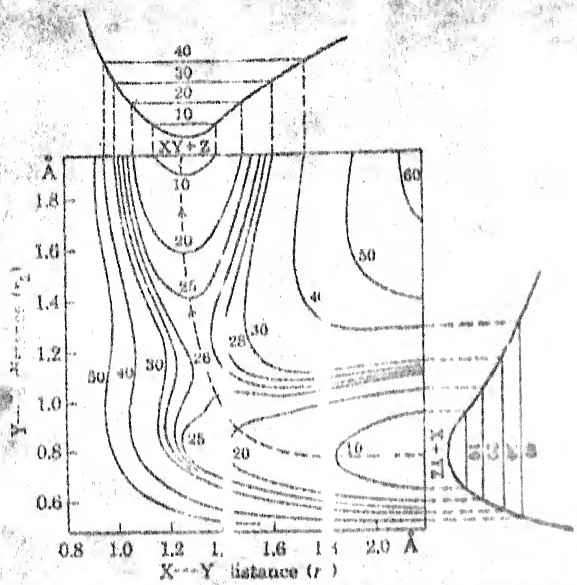

FIG. 8.—Typical potential energy surface for a three-atom reaction

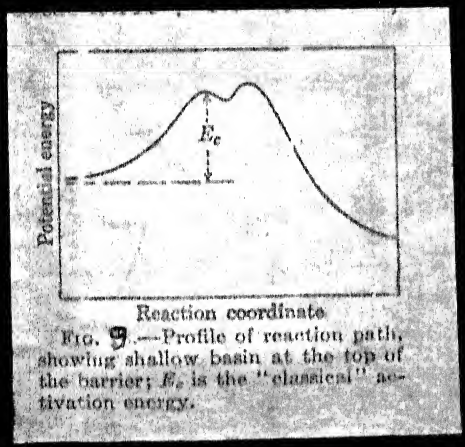

FIG. 9.—Profile of reaction path, showing shallow basin at the top of the barrier; E_c is the "classical" activation energy.

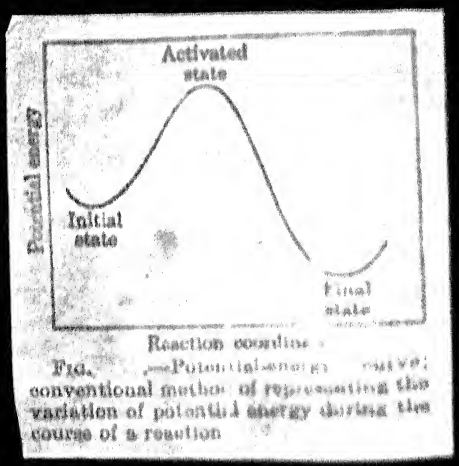

FIG. —Potential-energy curve; conventional method of representing the variation of potential energy during the course of a reaction

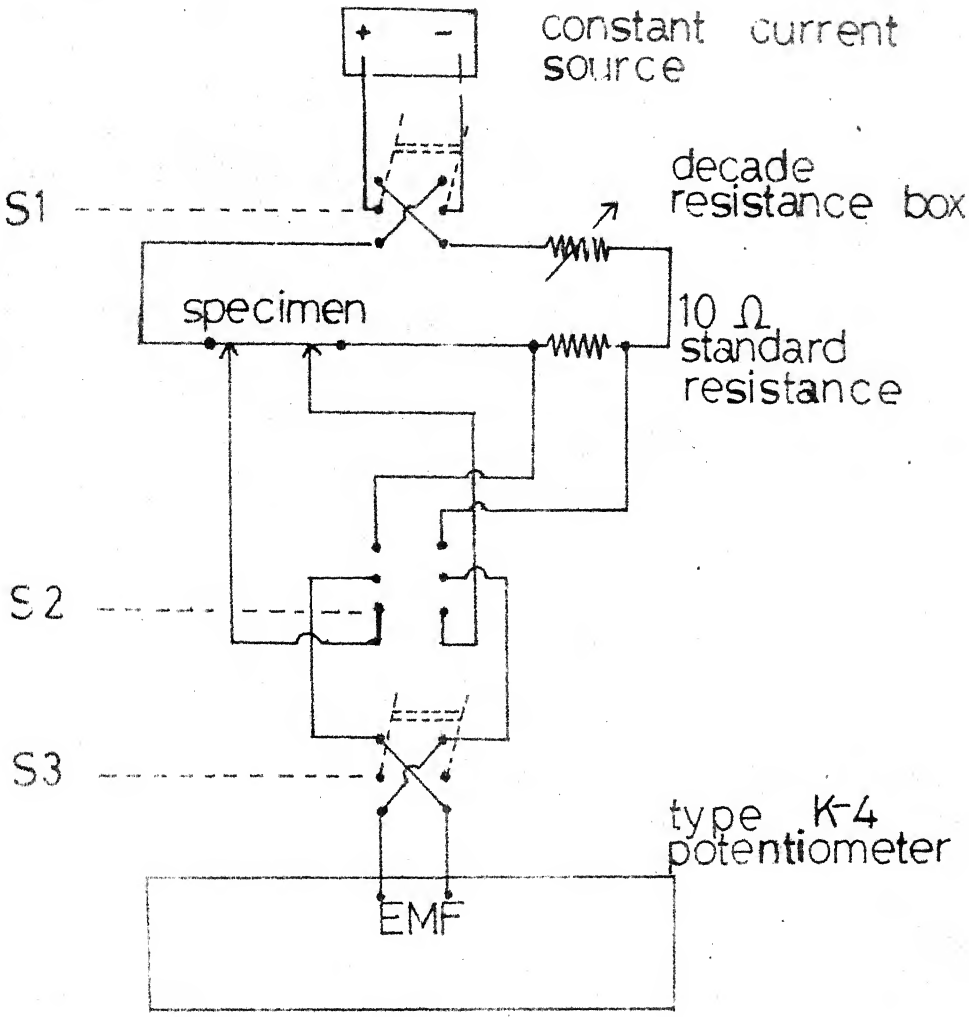

Fig.(10). Schematic of apparatus for measurement of electrical resistivity

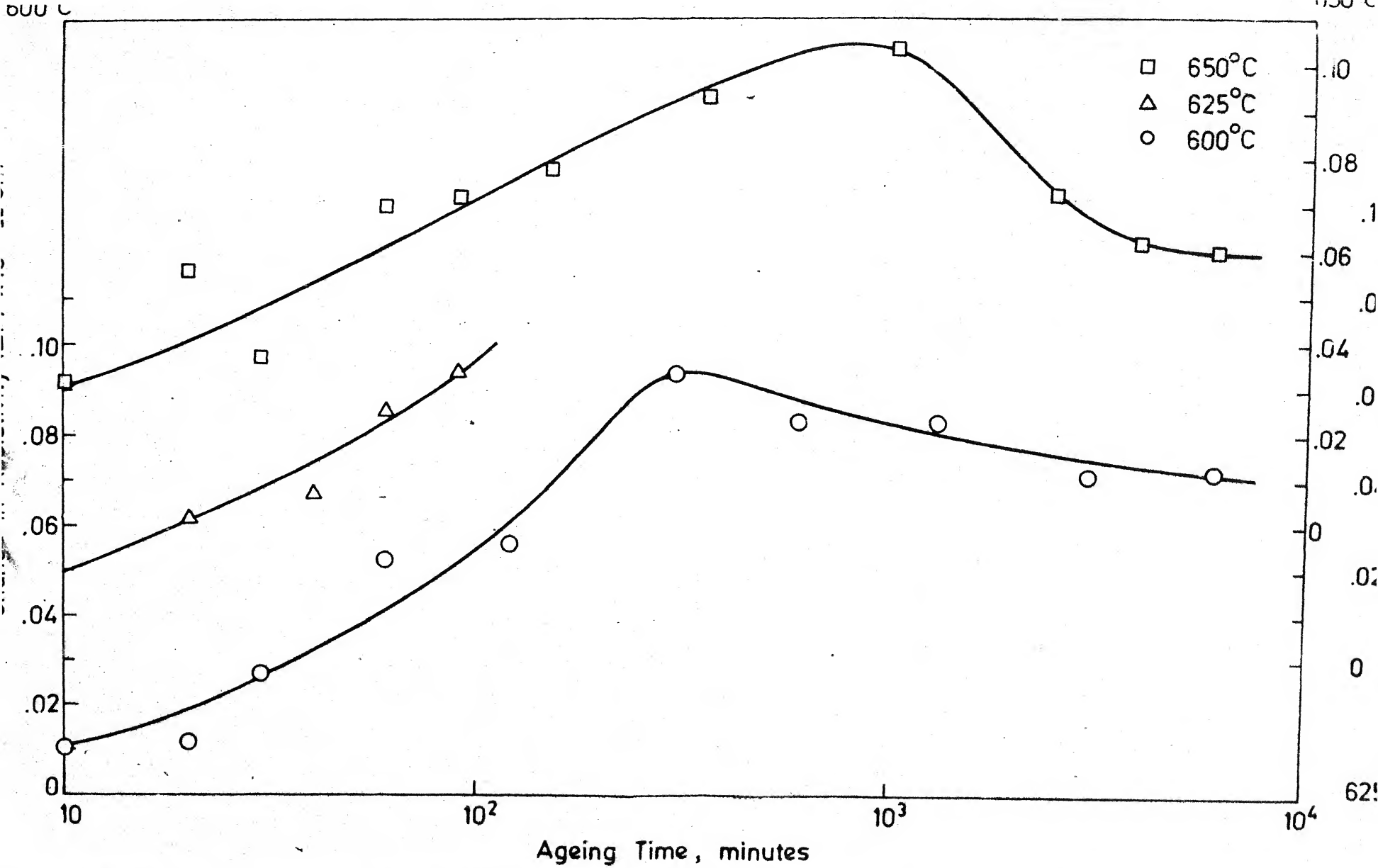

Fig 10 a Variation of Resistivity $\Delta\rho$ with Ageing Time at 600, 625 and 650°C.

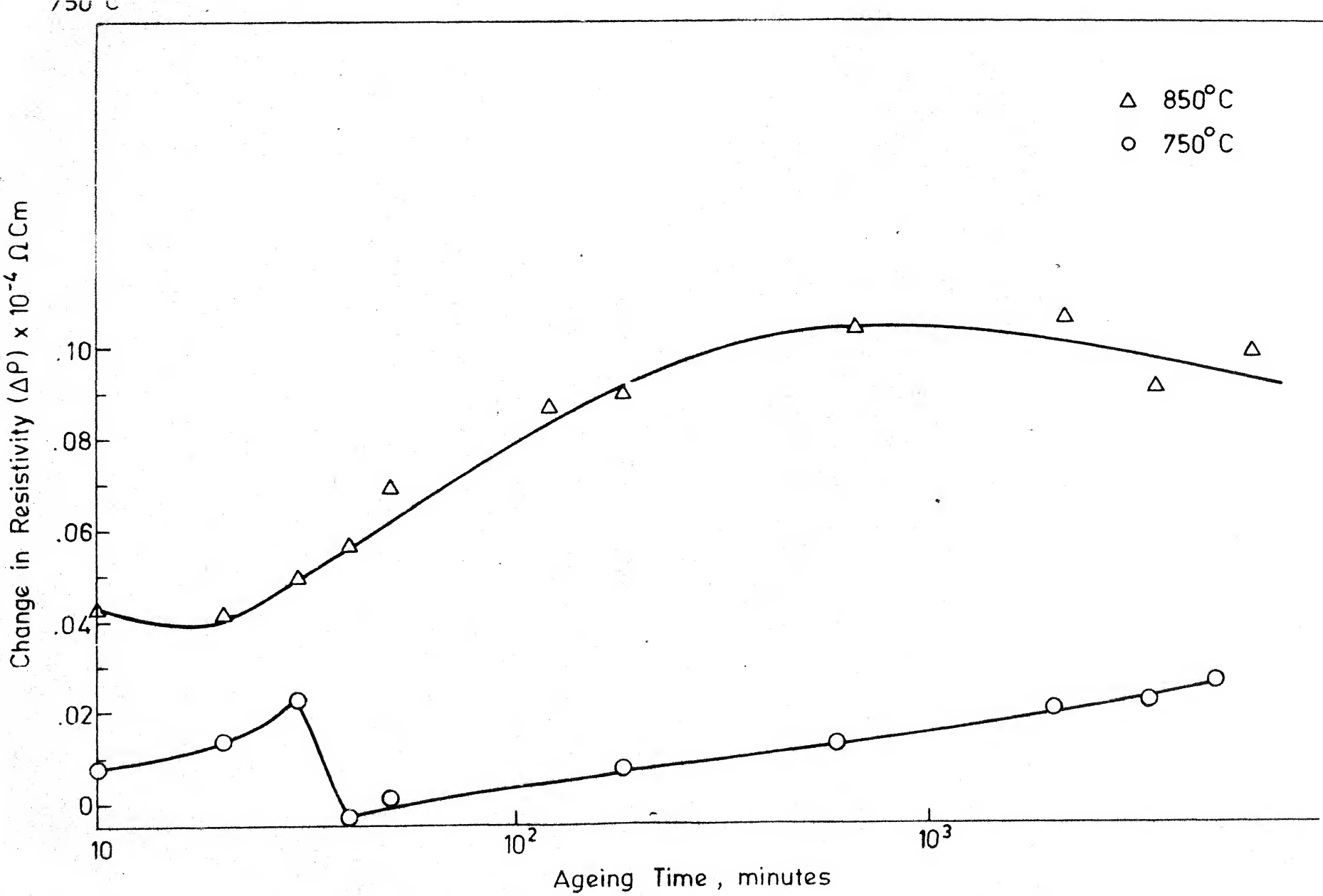

fig 10b Fig. (10b) Variation of Resistivity Δ P with Ageing Time at 750 and 850°C.

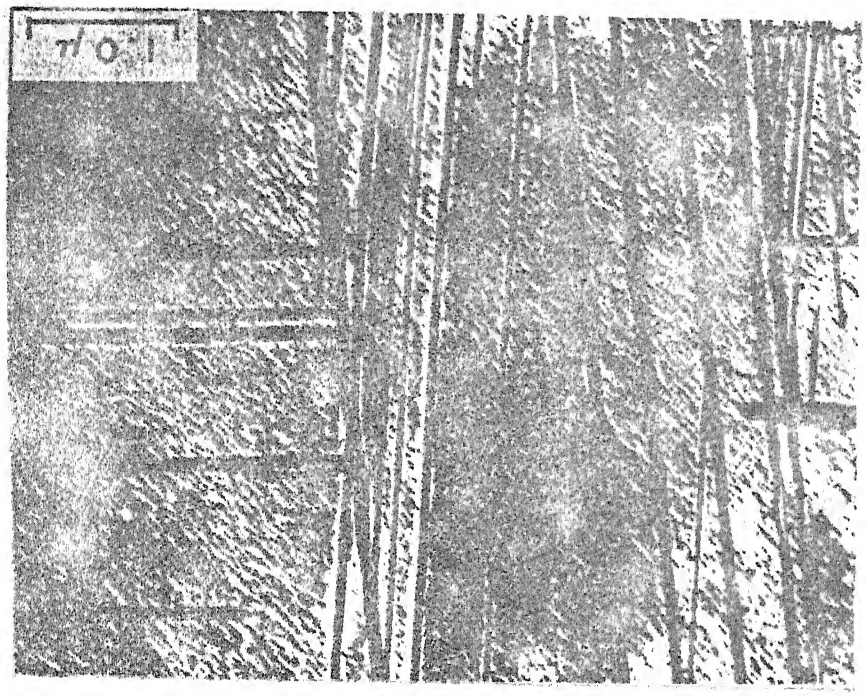

Fig. 10 c Structure of alloy aged for 50 hours at 750 c

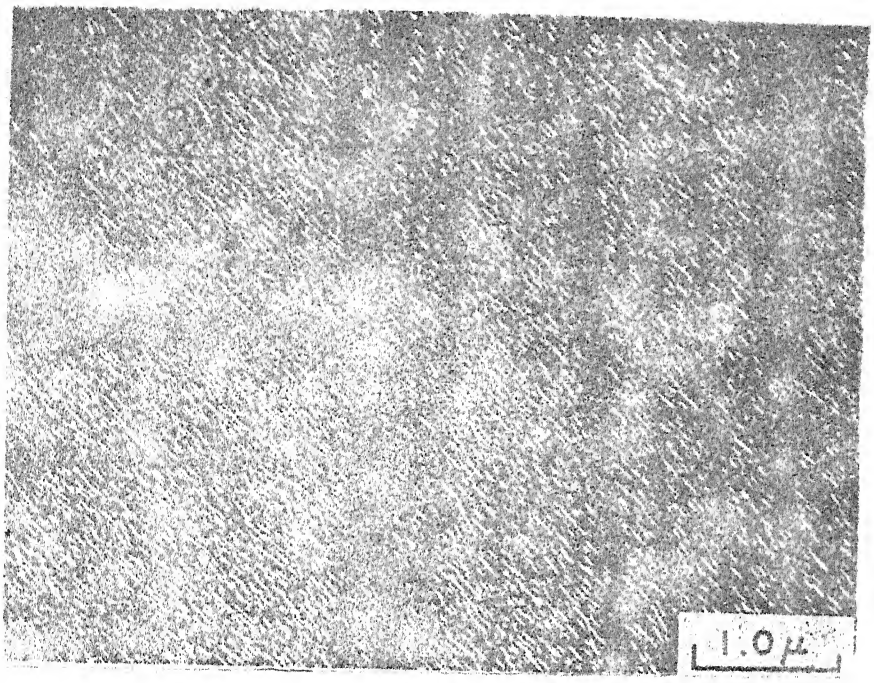

Fig 10d Dark field structure of γ'' precipitate present in fig 10c

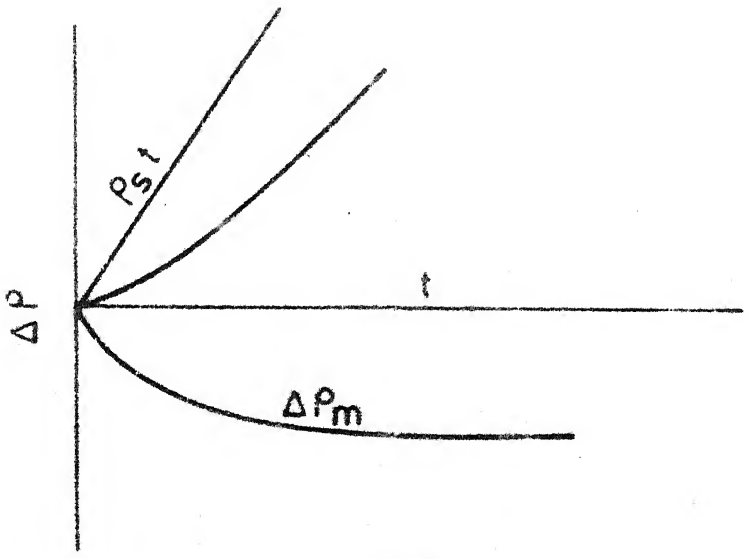

(a)

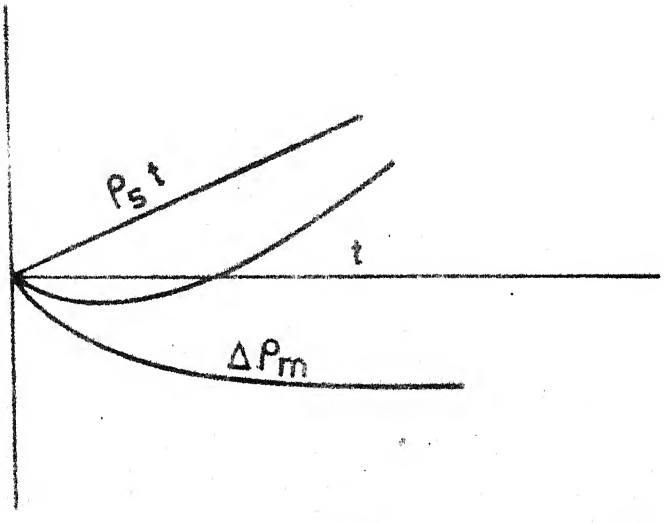

(b)

Fig. 11. Factors contributing to resistivity.

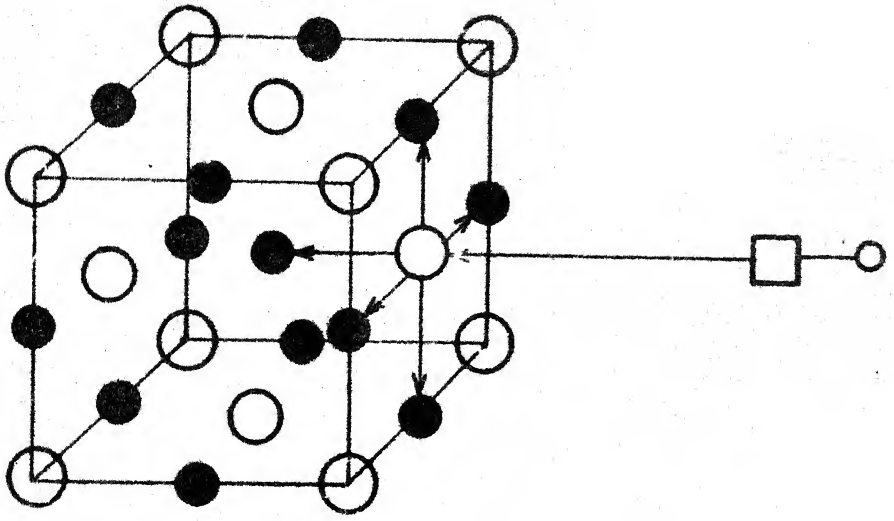

Fig. 12a FeO unit cell

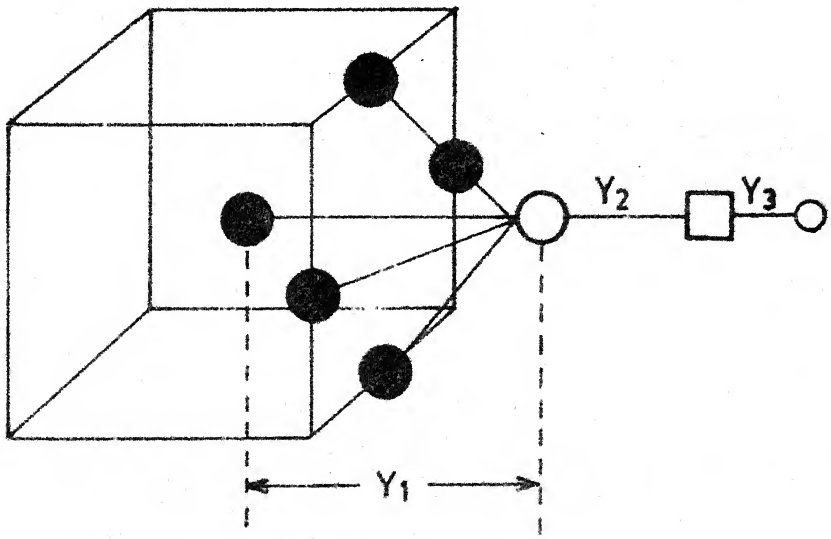

Fig. 12b Co intractions with FeO Lattice.

● Fe atoms

○ Oxygen atoms

□ Carbon atom

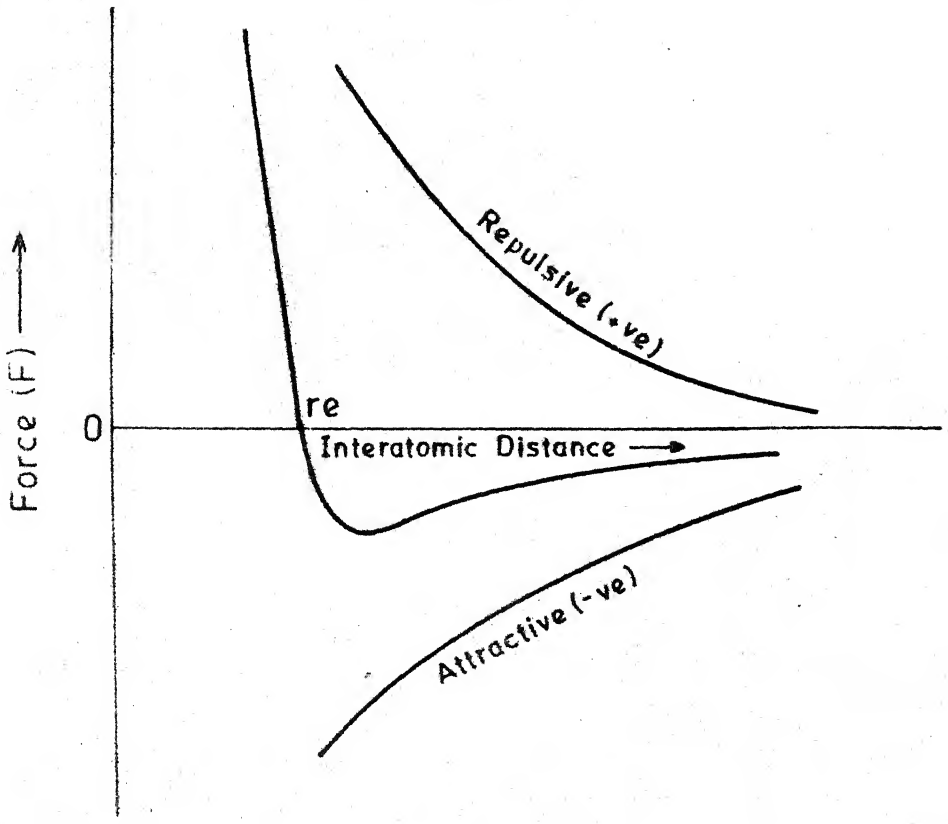

Fig. 13 Bonding beetween two atoms - Nature of Force

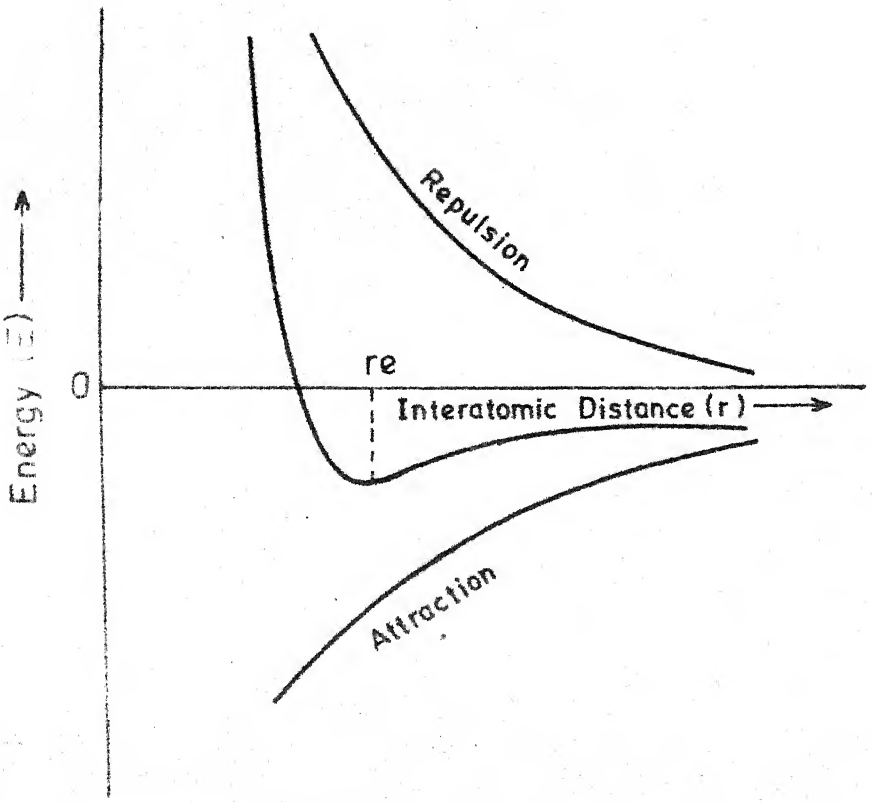

Fig 14 Bonding between two atoms - Nature of Energy.

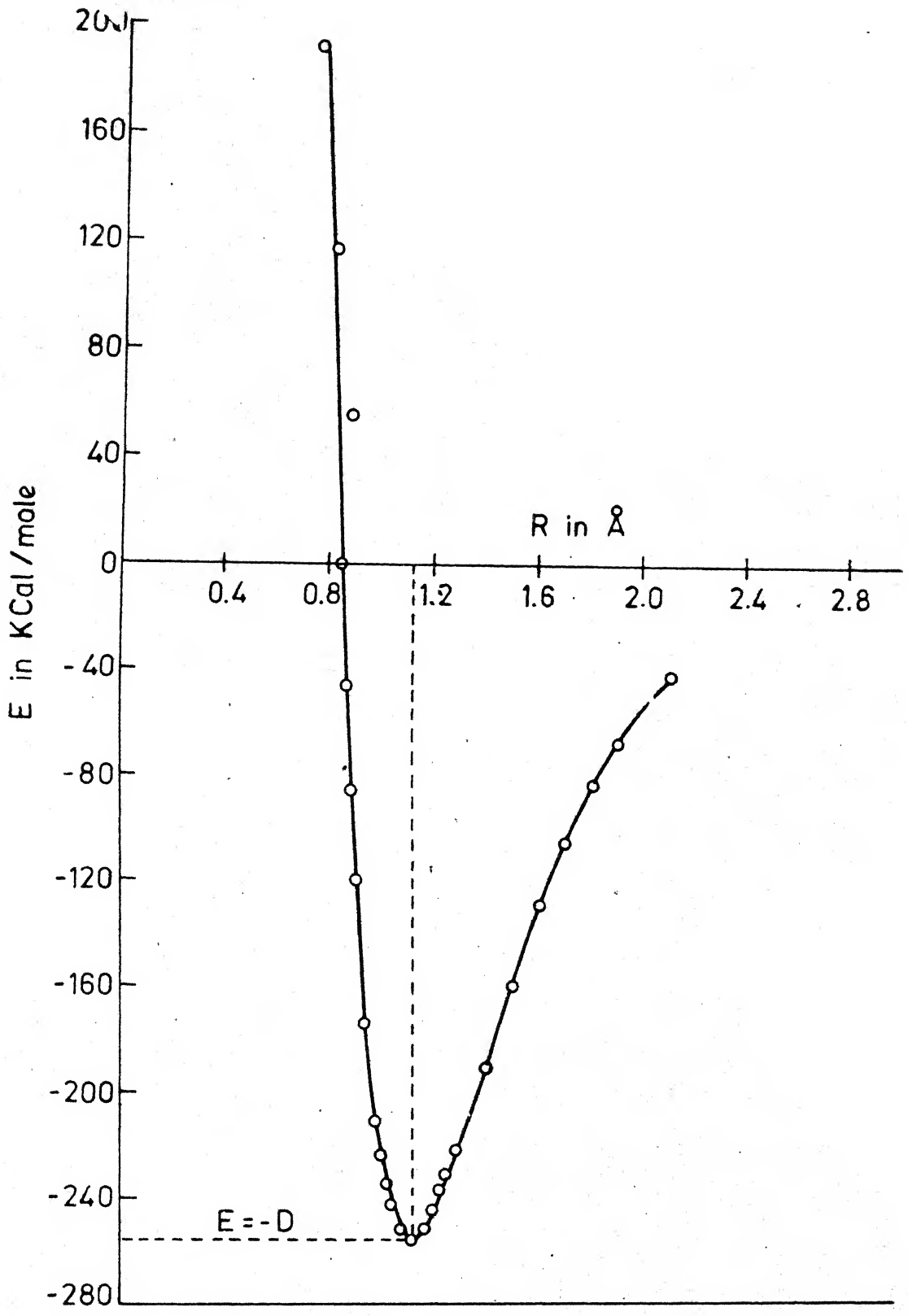

Fig.15 Potential energy curve for Diatomic molecule

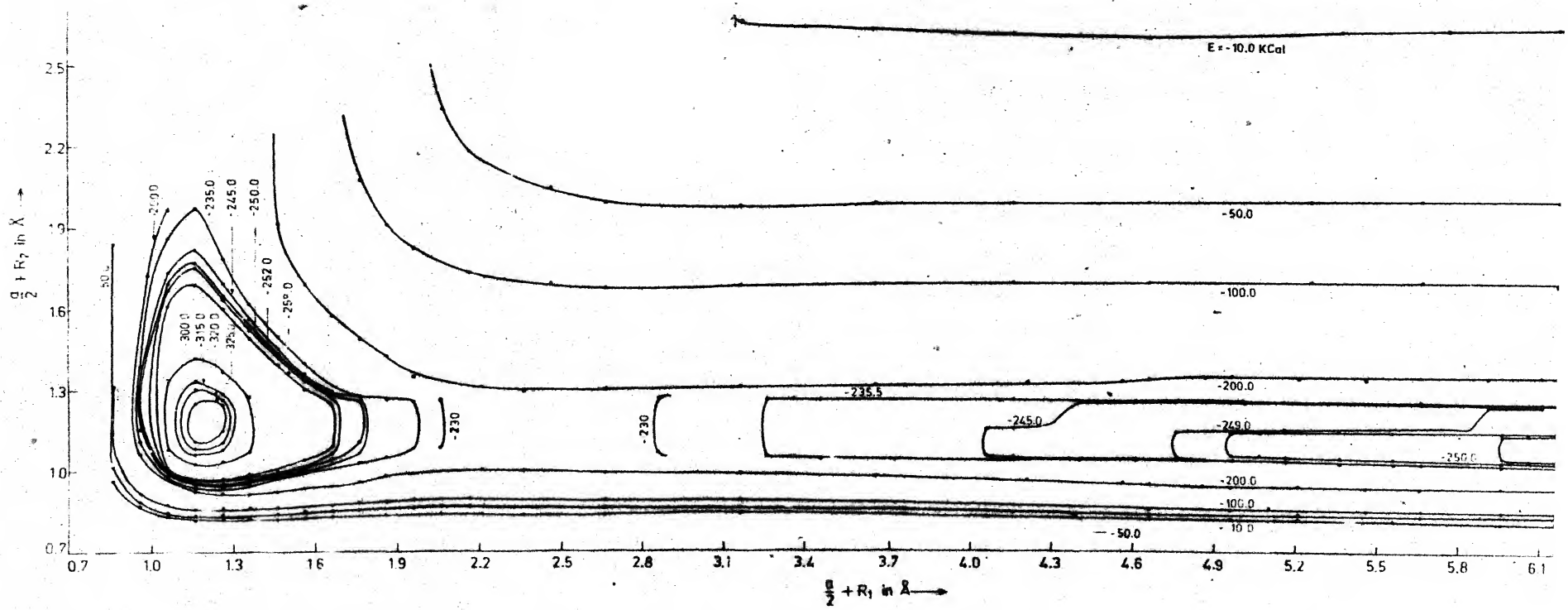

Fig.16 Potential energy contours for formation of CO_2 and CO and O

fig · 16

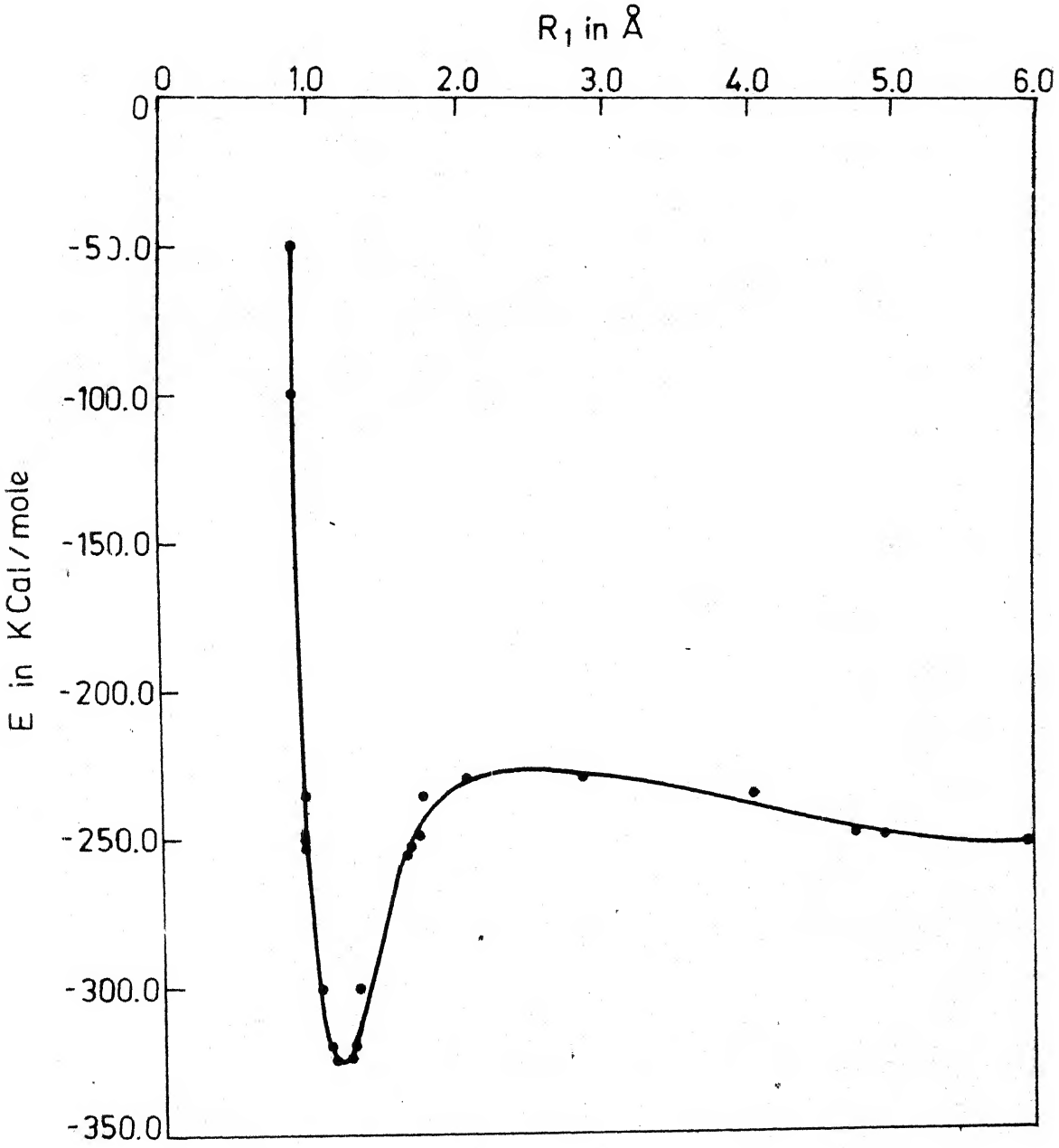

Fig. 17 Activation energy plot for CO_2

TABLE 1

RESISTIVITY OF SOLUTION TREATED SAMPLE

Sl.No.	HISTORY OF SAMPLE	RESISTIVITY x 10^{-4} Ω cm
1.	As Received, Solution Treated	1.324, 836 ± 0.003, 381
2.	Aged at 650°C, 100 hours and Solution Treated	1.338, 233 ± 0.001, 063
3.	Aged at 750°C, 30 minutes, Solution Treated, Aged at 750°C, 1 hour, Solution Treated	1.348, 782 ± 0.003, 279
4.	Aged at 750°C, 10 hours, Solution Treated	1.340, 720 ± 0.0003, 165
5.	Aged at 750°C, 82 hours, Solution Treated	1.336, 570 ± 0.0002, 570
6.	Aged at 850°C, 100 hours, Solution Treated. Aged at 700°C, 2 hours, Solution Treated	1.318, 360 ± 0.004, 690
7.	Aged at 600°C, 100 hours, Solution Treated	1.330. 595 ± 0.000, 745

TABLE 2

RESISTIVITIES OF AGED SAMPLES

Specimen Solution Treated at 1150°C for 1 hour.

Average of 3 Readings.

Average Resistivity = (1.318, 360 ± 0.004, 690) x 10^{-4} Ω cm

Temperature of Ageing = 600°C

Sl.No.	Ageing Time in minutes	No.of Readings	Average Resistivity (ρ) x 10^{-4} Ω cm	Change in Resistivity ($\Delta\rho$) x 10^{-4} Ω cm
1.	10	2	1.329, 805 ± 0.000, 285	0.011,445
2.	20	3	1.330, 103 ± 0.002, 764	0.011,743
3.	30	3	1.345, 743 ± 0.000, 349	0.027,383
4.	60	1	1.370, 490 ± 0.000, 000	0.052,130
5.	120	3	1.373, 863 ± 0.000, 328	0.055,503
6.	300	2	1.411, 465 ± 0.000, 015	0.093,105
7.	600	2	1.401, 100 ± 0.000, 000	0.082,740
8.	1320	2	1.401, 610 ± 0.000, 690	0.083,250
9.	3000	2	1.389, 640 ± 0.000, 390	0.071,280
10.	6000	2	1.390, 810 ± 0.000, 770	0.072,450

Specimen Solution Treated at 1150°C for 1 hour.

Average of 2 Readings.

Average Resistivity = (1.330, 595 ± 0.000, 745) x 10^{-4} Ω cm.

Temperature of Ageing = 625°C

Sl.No.	Ageing Time in minutes	No.of Readings	Average Resistivity (ρ) x 10^{-4} Ω cm	Change in Resistivity ($\Delta\rho$) x 10^{-4} Ω cm
1.	20	2	1.363, 435 ± 0.000, 725	0.032, 840
2.	40	2	1.368, 205 ± 0.000, 755	0.037, 610
3.	60	2	1.385, 835 ± 0.000, 765	0.055, 240
4.	90	2	1.395, 010 ± 0.000, 000	0.064, 415

Specimen Solution Treated at 1150°C for 1 hour.

Average of 3 Readings.

Average Resistivity = (1.324, 836 ± 0.003, 381) x 10^{-4} Ω cm

Temperature of Ageing = 650°C

Sl.No.	Ageing Time in minutes	No.of Readings	Average Resistivity (ρ) x 10^{-4} Ω cm	Change in Resistivity ($\Delta\rho$) x 10^{-4} Ω cm
1.	10	3	1.358, 558 ± 0.003, 273	0.032, 312
2.	20	3	1.381, 033 ± 0.002, 354	0.056, 197
3.	30	2	1.362, 527 ± 0.003, 202	0.037, 691
4.	60	1	1.394, 923 ± 0.000, 000	0.070, 087
5.	90	2	1.397, 509 ± 0.000, 359	0.072, 673
6.	150	2	1.403, 133 ± 0.000, 573	0.0782,975
7.	360	2	1.418, 067 ± 0.000, 309	0.093, 231
8.	1020	2	1.428, 067 ± 0.000, 235	0.103, 749
9.	2460	3	1.397, 023 ± 0.002, 053	0.072, 187
10.	3900	2	1.386, 862 ± 0.001, 500	0.062, 026
11.	6000	2	1.385, 606 ± 0.001, 038	0.060, 770

Specimen Solution Treated at 1150°C for 1 hour.

Average Resistivity = (1.34072 ± 0.003, 165) x $10^{-4}\Omega$ cm.

Temperature of Ageing = 750°C

Sl.No.	Ageing Time in minutes	No.of Readings	Average Resistivity (ρ) x $10^{-4}\Omega$ cm	Charge in Resistivity ($\Delta\rho$) x $10^{-4}\Omega$ c
1.	10	3	1.348, 406 ± 0.000, 585	0.007, 686
2.	20	2	1.354, 440 ± 0.001, 900	0.013, 720
3.	30	2	1.36 , 336 ± 0.000, 160	0.022, 640
4.	40	3	1.337, 220 ± 0.000, 686	-0.003, 500
5.	50	3	1.341, 940 ± 0.002, 540	0.001, 220
6.	180	2	1.347, 660 ± 0.001, 830	0.006, 940
7.	600	3	1.354, 466 ± 0.004, 748	0.013, 746
8.	2040	2	1.361, 110 ± 0.003, 720	0.020, 390
9.	3480	2	1.363, 310 ± 0.003, 620	0.022, 590
10.	4920	2	1.367, 130 ± 0.002, 700	0.026, 410

Speciman Solution Treated at 1150°C for ONE HOUR.

Average of 3 Readings.

Average Resistivity = (1.336, 570 ± 0.002, 570) x $10^{-4}\Omega$ cm

Temperature of Ageing = 850°C

Sl.No.	Ageing Time in minutes	No.of Readings	Average Resistivity (ρ) x $10^{-4}\Omega$ cm	Charge in Resistivity ($\Delta\rho$) x $10^{-4}\Omega$ cm
1.	10	3	1.328, 540 ± 0.004, 400	- 0.008,030
2.	20	2	1.327, 195 ± 0.000, 575	- 0.009,375
3.	30	2	1.335, 345 ± 0.001, 925	- 0.001,225
4.	40	3	1.343, 130 ± 0.004, 733	0.006,560
5.	50	2	1.355, 980 ± 0.002, 130	0.019,410
6.	120	3	1.373, 133 ± 0.000, 256	0.036,563
7.	180	2	1.375, 505 ± 0.003, 395	0.038,935
8.	660	3	1.390, 376 ± 0.000, 830	0.053,806
9.	2100	2	1.392, 370 ± 0.000, 770	0.055,800
10.	3480	2	1.378, 540 ± 0.001, 710	0.041,970
11.	6000	2	1.386, 430 ± 0.000, 340	0.049,860

TABLE

Parameters for the equation ( ) obtained by fitting it with values of ρ between 10 minutes to 120 of Ageing in the Present Work.

Sl. No.	Ageing Temperature °C	$K_1(S^{-1})$	$K_2(S^{-1})$	ρ_{Matrix} $\mu\Omega$ cm	ρ_i $\mu\Omega$ cm	ρ_s $\mu\Omega$ cm	ρ_l $\mu\Omega$ cm	Inve
1	600	0.1000×10^{-3}	0.9999×10^{-6}	129.63	11.5774	77933.4	-6.509×10^{6}	Pres
2	608	4.95×10^{-4}	3.33×10^{-6}	122.9	0.36	2.70	0.78	Whit
3	650	0.1500×10^{-3}	0.1240×10^{-9}	108.11	-16.1153	759.60	-5.623×10^{10}	Pres
4	653	1.97×10^{-3}	9.25×10^{-6}	121.72	1.7	2.93	1.18	Whit

REFERENCES

1. R.W. FAWLEY, in "The Super Alloys" edited by C.T.SIMS and W.C. HAGEL (John WILEY and SONS, NEW YORK,1972) p.3.

2. P.M. KELLY, Internat. Metallurgical Review Vol.18 (1973), p.31.

3. W.B. Pearson, "A Handbook of Lattice Spacings and Structures of Metals and Alloys" (Pargamon Press, OXFORD, 1967).

4. E.L. Raymond and D.A. Wells, in "SUPERALLOYS PROCESSING" (Metals and Ceramics Information Centre, Battelle, Columbus, Ohio, 1972).

5. R. Nordheim and N.J. Grant, Trans. A.I.M.E. Vol. 200, 1954, p. 211.

6. M.C. Chaturvedi and A.K. Jena, "The Effect of Vanadium Additions on the Precipitation Behaviour of Ni-CO-Cr-Nb-V Alloys", J. Mater. Sci. (in press).

7. D.W. Chung and M.C. Chaturvedi, "Effect of Fe Additions on the Precipitation Behaviour of Co Ni Cr Alloys Containing Nb", Met. Trans A, Vol.10A, Nov. 1979, p.1579.

8. J.C. Slater, "Introduction to Chemical Physics", Chapter XXII p. 377, MCGraw-Hill Book Company Inc., New York, 1939.

9. S. Glasstone, K.J. Laidler and H. Eyring , "Theory of Rate Processes", Chapter III, (McGraw Hill Book Company Inc., 1941).

10. R.J. White, S.B. Fisher, K.M. Miller and G.A. Swallow, "A Resistometric Study of Ageing in NIMONIC ALLOYS PE16", J. Nuclear Materials Vol.52 (1974) p. 51.

11. A. Adel and D.M. Dennison, "The Infrared Spectrum of Carbon Dioxide Part II", Physical Review, Vol.44, July 15, 1953, p. 99.

12. L.A.CIJRIFALCO and V.G.Weizer 'Application of the Morse Potential function to Cubic metals' physical Review, vol 14, no.3, May 1;1959 P687.